Hyperfine Interactions 123/124 (1999) 31–77

General properties of nuclear resonant scattering

G.V. Smirnov

Russian Research Center 'Kurchatov Institute', Kurchatov Square 1, 123182 Moscow, Russia
E-mail: smirnov@polyn.kiae.su

The process of nuclear resonant scattering is considered on the basis of an optical model. The coherent properties of the radiation and scattering mechanism are described. The complementary pictures of γ-ray resonant scattering in energy and time domains are presented. Special attention is paid to scattering of a γ quantum by an ensemble of nuclei. The central concept of the theory of nuclear resonant scattering, the nuclear exciton, as a delocalized nuclear excitation, is described in detail. It is shown that both temporal and spatial aspects of coherence play a crucial role in the evolution of the nuclear exciton. A large place is given to the analysis of resonant scattering of synchrotron radiation by nuclear ensembles.

1. Introduction

For a long time the impact of ideas of coherency and scattering on the art and science of Mössbauer spectroscopy was not very essential. The main line of development of Mössbauer experiments was in the frame of absorption spectroscopy. Mössbauer physicists dealt mostly with absorption spectra taken either in traditional transmission experiments or in measurements of conversion electron yield or some other secondary radiation.

For the interpretation and description of these spectra it was appropriate to use the picture of interaction of a γ-quantum with an individual nucleus exploiting the nuclear resonant absorption cross-section. The coherent properties of radiation and those of the interaction mechanism were not explicitly involved.

Nevertheless, already at an early stage of the Mössbauer era scattering experiments clearly proved the coherence of Mössbauer radiation and of nuclear scattering. Coherent phenomena with Mössbauer γ-rays were thoroughly investigated. These studies over about thirty years formed the basis of a new branch of optics (for an overview of experiments and theory see [1–7] and references therein).

The development of synchrotron radiation sources, particularly of third generation facilities, brought to life the potential of all this knowledge. Now, with the increasing application of synchrotron radiation sources for studying nuclear resonances [8–15] the ideas and approaches of coherence physics turn out to be of great importance for understanding and describing of the results of measurements. The interest in the new field is rising. To make a bridge for entering as a Mössbauer spectroscopist the new area we consider in this paper the general properties of nuclear resonant scattering

involving the principles and notions of the optical theory. Emphasis will be given to the *interferometric aspects of the new method, which make it complementary to Mössbauer absorption spectroscopy*.

2. Coherent properties of radiation

2.1. Wave packet description of Mössbauer quanta

Let us consider a radiative transition between the first excited and the ground nuclear state with energies E_1 and E_0. To describe the γ-radiation we use classical electromagnetic theory. It is an approximation of quantum electrodynamics, which may be applied to our case. The wave–particle duality of γ-radiation associates the probability wave language for the description of a γ-quantum state with that using electromagnetic fields. So the probability amplitude for finding a quantum can be associated with the relevant electric field strength in the wave train. In case of recoilless emission the multipolarity, the polarization, the frequency and the decay rate of the γ-ray field emitted during the nuclear transition are determined precisely by the multipole moment of the nuclear transition. Since the size of a nucleus carrying a transition moment is much less than the radiation wavelength, a nucleus can be treated as a point emitter. In the absence of hyperfine splitting of the nuclear levels the nucleus emits a spherically symmetric wave packet so that the electric field vector at the point of observation given by the vector **r** from the origin and at time t is of the form

$$\mathbf{E} = \mathbf{const} \cdot \frac{1}{r}\, \mathrm{e}^{\mathrm{i}(\omega_\mathrm{s} t - \mathbf{kr}) - \Gamma t/2\hbar}, \quad t \geqslant 0, \tag{2.1}$$

where $t = 0$ is the time of the formation of the excited state, $\omega_\mathrm{s} = (E_1 - E_0)/\hbar$ is the wave packet carrier frequency, Γ is the natural width of the excited nuclear level, which is related to the characteristic decay time t_0, $\Gamma t_0 = \hbar$, and **k** is the propagation vector giving the wavelength λ by $k = 2\pi/\lambda$, and the direction of propagation. The electric field oscillates in space and in time. Its *oscillation phase* contains both temporal and spatial parts: $\omega_\mathrm{s} t - \mathbf{kr}$.

The notion of coherence for an electromagnetic field implies a correlation of the phase of the oscillation of the electric and magnetic fields in space and in time. Any Mössbauer nucleus presents a source of highly coherent radiation. The phase correlation of the electric field of the γ-ray at the point of observation extends typically over times of 10^{-9}–10^{-5} s. For the most frequently used ^{57}Fe nucleus this corresponds to $\approx 5 \cdot 10^{11}$ cycles of the field oscillation. Alternatively one may say that the coherent γ-ray wave train extends over $\approx$30 m! In the simplest interpretation one may equate the *coherence length* to the length of the photon wave train.

Any photon wave train can be represented as a coherent superposition of time–space harmonic plane waves (i.e., of spectral–spatial field components)

$$\mathbf{E}(\mathbf{r}, t) = \mathbf{e} \cdot \varepsilon_\omega\, \mathrm{e}^{\mathrm{i}(\omega t - \mathbf{kr})}, \tag{2.2}$$

where ω is the wave frequency, **e** is the unit vector of the wave polarization (in general, a complex vector: $\mathbf{e} = \mathbf{e}_1 + \mathrm{i}\mathbf{e}_2$, where all **e**-vectors are normal to **k**), ε_ω is the scalar amplitude (in general, a complex number[1]) of the constituent wave at frequency ω. Note that the double harmonic plane wave given by eq. (2.2) is an ideal physical concept of the wave field where the phase correlation spreads infinitely in space and in time.

The electric field amplitude of a γ-ray emitted without recoil in a nuclear transition can be decomposed into time harmonics (spectral or frequency components) by means of a Fourier expansion of the time dependent exponential in eq. (2.1),

$$E(t) \propto \mathrm{e}^{\mathrm{i}(\omega_\mathrm{s}+\mathrm{i}\Gamma/2\hbar)\,t}\Theta(t) = \mathrm{const}\int_{-\infty}^{\infty} \mathrm{d}\omega \cdot \varepsilon_\omega\, \mathrm{e}^{\mathrm{i}\omega t}, \tag{2.3}$$

where $\Theta(t)$ is the unit step function, which is zero for negative argument (the formation of the nuclear excited state is supposed to occur at $t = 0$). Multiplying eq. (2.3) by $\exp(-\mathrm{i}\omega' t)$ and integrating over time from $-\infty$ to $+\infty$ yields the following expression for the amplitudes of the spectral components:

$$\varepsilon_\omega = \mathrm{const} \cdot \frac{1}{\omega - \omega_\mathrm{s} - \mathrm{i}\Gamma/2\hbar} \tag{2.4}$$

(where ω' is replaced by ω). This expression corresponds to a Lorentzian energy distribution characterized by the width Γ. All spectral components $\varepsilon_\omega \exp(\mathrm{i}\omega t)$ are coherent by construction. The integration at the right-hand side of eq. (2.3) physically means interference of the time harmonic oscillations. The result is determined by the frequency distribution of $|\varepsilon_\omega|$ and by the evolution of the phases of the spectral components with time. One may say that eq. (2.3) when read from right to left presents *a transition from the frequency to the time domain in the description of a γ-ray*. In our case the interference of the spectral components yields a fading oscillation with carrier frequency ω_s and decay constant $\Gamma/2\hbar$. Thus the coherence time and the coherence length of the real photon wave train are intimately connected with the width of the spectral distribution of its harmonic components.

2.2. Description of the synchrotron radiation wave packet

An electron orbiting in a storage ring radiates when it is accelerated in a bending magnet, or an undulator. An extremely short wave train of synchrotron radiation (SR) is emitted, which lasts for about 10^{-18} s and is of 10^{-10} m length. The relevant spectrum of electromagnetic radiation spreads from visible light to hard X-rays with the upper limit extending up to $\sim$100 keV. The energy range thus covers the nuclear transitions of almost all Mössbauer isotopes. The X-rays generated in an undulator-based SR source can have an especially high spectral density in particular in the region of nuclear resonances.

[1] One should remember that mathematically it is convenient to operate with the electric field amplitude as a complex vector but only its real part has a physical meaning.

Before striking the nuclear target the SR light passes through a monochromator system which selects a limited band of radiation, $\hbar\Delta\omega$ ($\hbar\Delta\omega$ usually lies in the eV–meV range). It is very narrow with respect to the primary spectrum of SR but extremely broad compared to the width of a nuclear resonance. In practice one may assume that all spectral components of the incident radiation have equal amplitudes within the selected band, i.e., $\varepsilon_\omega = \varepsilon_{\omega_0}$ (ω_0 is the frequency of the nuclear transition). Thus, the radiation spectrum at the exit of the monochromator is represented by a continuous set of coherent harmonics

$$E(\omega, t) = \varepsilon_{\omega_0}\, \mathrm{e}^{\mathrm{i}\omega t} \quad \text{with } \varepsilon_{\omega_0} = \sqrt{I_0/\Delta\omega}, \tag{2.5}$$

where the amplitude ε_{ω_0} is frequency independent in contrast to the amplitude ε_ω of Mössbauer radiation according to eq. (2.4), I_0 is the intensity of SR within the frequency range $\Delta\omega$ selected by the monochromator system.

Electrons are grouped in bunches of finite size in a storage ring. Since the bunch size significantly exceeds the wavelength of X-radiation the wave packets from separate electrons cannot be regarded as coherent and their intensities are added in the signal resulting at the detector.

After looking at the coherent properties of radiation we turn to the description of the scattering mechanism.

3. Elastic scattering by a single nucleus

3.1. Steady state and dynamic picture of scattering

The overall process – absorption of a γ-ray or an X-ray photon by a nuclear target and the re-radiation of a photon – is a scattering process. Due to the interaction with the target the amplitude distribution, the polarization state, the form of the wave front, etc. of the incoming photon can be radically transformed. The task of a scattering theory is to give the full picture of the photon wave packet transformation, which is determined by the properties of the scattering mechanism and by the parameters of the scattering system. In resonant scattering, particularly, the change of the spectral components of the wave packet is of special concern. There are different approaches possible to describe the effect of scattering (so far we assume the polarization state and the direction of scattering to be unchanged).

The most universal approach is to describe the transformation of a separate time harmonic component of the wave packet, i.e., the change of its amplitude and phase due to resonant scattering. In this description the response of a scattering system to a harmonic excitation, i.e., the *steady state response*, at each frequency in the range of interest is calculated. The scattering process is described here in the *frequency domain*. When the transformed components are determined one gets by their superposition the unit wave packet emerging from the scattering system.

In another approach the emerging wave packet can be found directly if the *free dynamic response* of the nuclear system is known, say, the response of a resonating

system to a pulsed excitation. In this approach the resonant scattering is described in the *time domain*.

SR sources provide an excellent opportunity to observe the time evolution of nuclear scattering. The excitation of a nuclear target by a SR pulse occurs within $\sim$0.2 ns. The time response of nuclei, e.g., short-lived isomers used in Mössbauer spectroscopy, lies in the microsecond range. Thus, the excitation and decay stages are well separated in time and the decay is so long that it can be easily traced with modern electronics.

Below we consider both of the mentioned approaches.

3.2. Frequency response of a bound nucleus

The response of a nucleus is given by the nuclear scattering amplitude. The incident quantum excites the nuclear transition in which the nucleus behaves as an oscillating multipole that radiates. Usually an ensemble of nuclei participates in the scattering event and the scattering amplitude is derived as a quantum mechanical average over this ensemble. We limit our discussion to *elastic forward scattering* of γ-rays by a bound nucleus with vanishing hyperfine interaction. In this case we may consider the scattering amplitude as a *complex function* $f_0(\omega)$, which *relates the amplitudes and phases of the relevant frequency components of the incident and scattered radiation*

$$E_{\mathrm{s}}(\omega) = f_0(\omega) \cdot E_{\mathrm{i}}(\omega), \tag{3.1}$$

where the scattering amplitude as a function of frequency is

$$f_0(\omega) = -\frac{K}{4\pi} \cdot \sigma_0 \cdot \frac{\Gamma/2\hbar}{\omega - \omega_0 - \mathrm{i}\Gamma/2\hbar} \cdot f_{\mathrm{LM}}(\mathbf{K}) \cdot \beta. \tag{3.2}$$

$f_0(\omega)$ can be interpreted as the response function of an isolated nucleus in the frequency domain. In eq. (3.2)

$$\sigma_0 = \frac{2\pi}{K^2} \cdot \frac{1}{1+\alpha} \cdot \frac{2I_{\mathrm{e}}+1}{2I_{\mathrm{g}}+1}$$

is the maximum resonance cross-section, $\Gamma = \Gamma_\gamma + \Gamma_{\mathrm{e}}$ is the natural width of the nuclear excited level composed of radiative and radiationless parts (the energy of the excited nucleus can also be lost by ejecting an atomic electron via internal conversion), $\alpha = \Gamma_{\mathrm{e}}/\Gamma_\gamma$ is the internal conversion coefficient and I_{e}, I_{g} are the nuclear spins of the ground and excited states (in the case of the ^{57}Fe nucleus $\sigma_0 = 2.56 \times 10^{-18}$ cm^2, $\alpha = 8.19$, $\Gamma = 5 \cdot 10^{-9}$ eV, $I_{\mathrm{g}} = 1/2$, $I_{\mathrm{e}} = 3/2$), $K = \omega/c$ is the magnitude of the γ-ray wave vector in free space, $f_{\mathrm{LM}}(\mathbf{K}) = \exp\{-\langle(\mathbf{Ku})^2\rangle\}$ is the Lamb–Mössbauer factor representing the recoilless fraction of the scattered radiation ($\mathbf{u}$ is the displacement of the nucleus from its equilibrium position due to thermal vibrations) and β is the isotopic enrichment of the target.

As a complex number the scattering amplitude may be written in the form $f_0 = |f_0(\omega)| \exp\{\mathrm{i}\Phi(\omega)\}$, where $|f_0(\omega)|$ represents the attenuation of the amplitude of the

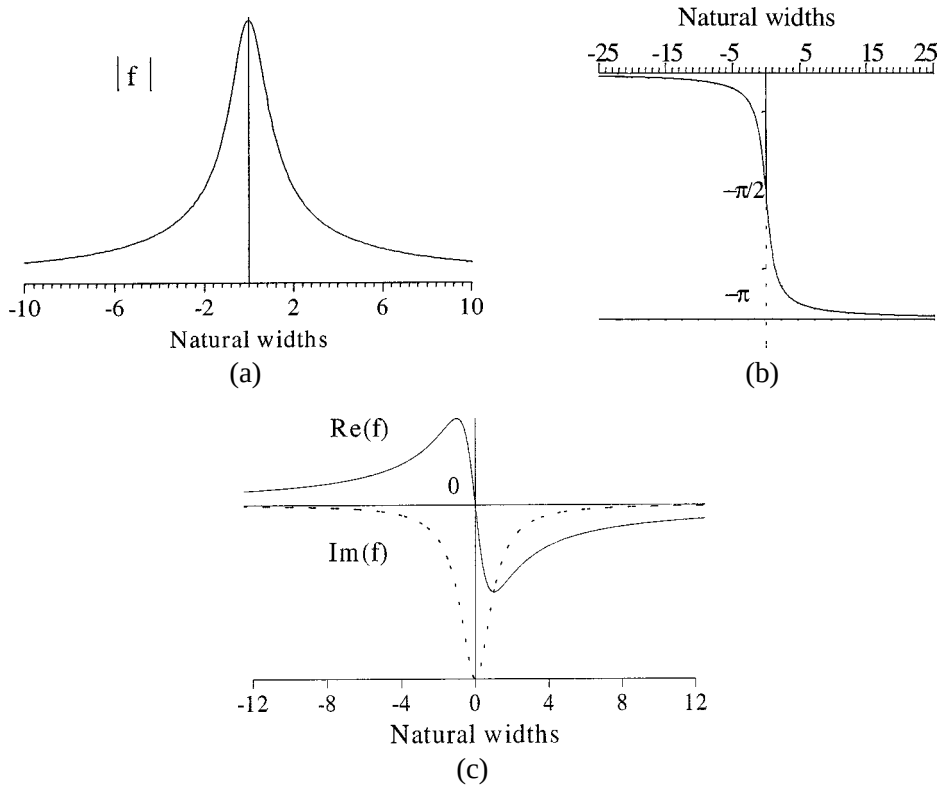

Figure 1. The amplitude of the elastic scattering by a bound nucleus in the forward direction. The magnitude (a), the phase (b), the real and imaginary parts (c) of the forward scattering amplitude in the vicinity of the resonance energy.

scattered radiation component and $\Phi(\omega)$ is the phase shift of the radiation component gained in forward scattering. In figure 1 the scattering amplitude in the resonance region is given.

Dramatic changes of the scattering amplitude occur in the vicinity of a resonance, within a few natural nuclear level widths (only $\approx 2 \cdot 10^{-8}$ eV in the case of ^{57}Fe). The amplitude is sharply peaked at resonance, figure 1(a), and the phase drops from zero below the resonance to $-\pi$ above the resonance and is $-\pi/2$ at resonance, figure 1(b).

It is convenient to operate with the imaginary and real parts of the scattering amplitude: $f_0(\omega) = \mathrm{Re}[f_0(\omega)] + \mathrm{i}\,\mathrm{Im}[f_0(\omega)]$ as shown in figure 1(c). *At resonance the amplitude is purely imaginary, but on the wings* $|\mathrm{Re}(f_0)| \gg |\mathrm{Im}(f_0)|$ *so that the amplitude is almost real*. As we shall see below, this property of the scattering amplitude plays a crucial role in the formation of a specific frequency structure of the γ-ray wave packet coherently scattered by the nuclear ensemble.

3.3. *From frequency to time response of a nucleus*

In figure 2 the scattering of a SR X-ray wave packet is displayed schematically. The upper panel shows the incoming wave packet, the bottom panel shows the outgoing one. The left/right-hand columns present the steady state and the dynamic picture of scattering, respectively.

The incoming radiation, approximated by a $\delta(t)$ function, can be decomposed into a continuous set of oscillations of equal amplitude over an infinite frequency range, (figure 2 – see the upper left-hand corner). The components of the SR are displayed as arrows (bold lines) in the complex plane determined by the axes Im(E), Re(E). The arrows are distributed along the ω-axis, and each arrow is rotating with its angular frequency ω in the complex plane. At time zero they are all aligned in one direction, i.e., they are all in phase producing a resultant sum with infinite amplitude, at all other times they are smeared homogeneously in phase over 2π yielding zero amplitude, in full agreement with the properties of a δ-function.

The amplitudes and the phases of the elementary oscillations are changed due to resonant scattering according to eqs. (3.1) and (3.2). In contrast to the incoming

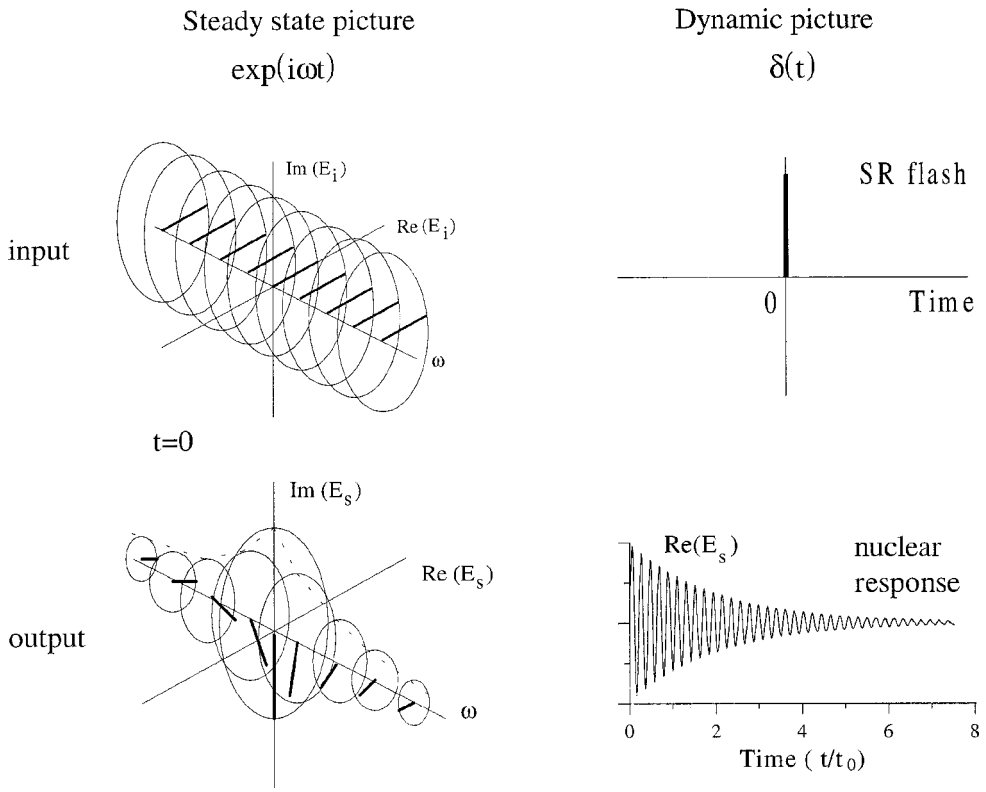

Figure 2. Schematic view of nuclear resonant scattering of a SR X-ray wave packet in the energy and time domains.

set of amplitudes the amplitudes of outgoing oscillations are peaked at the resonance frequency within a narrow band determined by the resonance width, and their initial phases are dispersed around $-\pi/2$, see figure 2 (bottom left). When all scattered waves are summed to a unit wave packet the nuclear response in the time domain is obtained (bottom right). Geometrically this means that the vector summation of all arrows in figure 2 (bottom left) is performed. The dephasing of the elementary oscillations (due to rotation of the arrows at different angular frequencies) results in a decay of the wave packet amplitude. The sharper the resonance the slower the dephasing and the response time of a nucleus is correspondingly larger.

Thus the decay of the scattering intensity can be interpreted as a fading of the interference signal due to the frequency components becoming homogeneously distributed in phase with time. Analytically one has to perform the integration of $E_{\rm s}(\omega, t)$ in the frequency domain. Taking into account eqs. (2.5) and (3.1) we have

$$E_{\rm s}(t) = \varepsilon_{\omega_0} f_0(t), \quad \text{where} \quad f_0(t) = \frac{1}{2\pi}\int_{-\infty}^{\infty} {\rm d}\omega \cdot f_0(\omega)\, {\rm e}^{{\rm i}\omega t}. \tag{3.3}$$

After substitution of eq. (3.2) into eq. (3.3) we obtain

$$f_0(t) = -\frac{K}{4\pi}\sigma_0 f_{\rm LM}\beta \frac{1}{2\pi}\int_{-\infty}^{\infty} {\rm d}\omega \frac{\Gamma/2\hbar}{\omega - \omega_0 - {\rm i}\Gamma/2\hbar}{\rm e}^{{\rm i}\omega t}. \tag{3.4}$$

The integrand in eq. (3.4) has a singularity in the upper half of the complex ω plane at $\omega = \omega_0 + {\rm i}\Gamma/2\hbar$. The integral can be evaluated by closing the contour on a semicircle in the upper part of the plane and finding the residue of the integrand. Thus, we obtain for the *scattering amplitude as a function of time*

$$f_0(t) = -{\rm i}\frac{K}{8\pi} \cdot \sigma_0 f_{\rm LM}\beta \frac{1}{t_0}{\rm e}^{{\rm i}\omega_0 t - t/(2t_0)}\Theta(t), \tag{3.5}$$

where $t_0 = \hbar/\Gamma$ (for $\Theta(t)$ see eq. (2.3)).

We can conclude that due to nuclear scattering the initial δ-function wave packet is transformed into an exponentially decaying oscillation at the carrier frequency of the nuclear resonance, $f_0(t)$ thus *represents the response function of an isolated nucleus in the time domain*.

In this section the dynamic response of a scatterer was found by using its frequency response. For that the transition from the time domain to the frequency domain and back via the Fourier transformations was made, presented schematically in figure 2: counterclockwise transition from upper right to lower right corner.

3.4. Response function technique

However, when the time response function of a scattering system is known one can avoid addressing the frequency domain and describe the transformation of an

arbitrarily shaped wave packet directly in the time domain with the aid of the response function technique given by

$$E_{\rm s}(t) = \int_{-\infty}^{\infty} {\rm d}t' R\big(t-t'\big) E_i\big(t'\big), \tag{3.6}$$

where $E_i(t')$ represents the wave packet of a γ-ray incident on the target, $E_{\rm s}(t)$ represents the scattered wave packet, $R(t-t')$ is the time response function of the target, t' and t are the excitation and the de-excitation times, respectively. The probability amplitude for the overall scattering event can be understood as the product of the probability amplitudes of two sequential events, the excitation and the de-excitation, integrated over all possible excitation times.

To illustrate the response function technique we describe the multiple nuclear scattering of a SR X-ray. We have already found the wave packet scattered by a single nucleus, see eqs. (3.3)–(3.5), and figure 2 the lower right. Next we consider the scattering of this γ-ray by a second nucleus. This nucleus is exposed to the field of the γ-ray in the time interval $(0, +\infty)$ and decays within the same time interval. Thus it exhibits a driven oscillation rather than a free one (like in the first scattering). The second scattering is represented by the integral of eq. (3.6), where the wave packet $E_i(t')$ now has the time structure given by eq. (3.5), and the response function is $R = f_0(t-t')$, thus the integral in eq. (3.6) is

$$\int_{-\infty}^{\infty} {\rm d}t' \exp\left\{ {\rm i}\omega_0\big(t-t'\big) - \frac{(t-t')}{2t_0} \right\} \Theta\big(t-t'\big) \exp\left\{ {\rm i}\omega_0 t' - \frac{t'}{2t_0} \right\} \Theta\big(t'\big).$$

Performing the integration we obtain the following wave packet for the double scattered SR X-ray:

$$E_{\rm s}(t) \propto (-t) {\rm e}^{{\rm i}\omega_0 t - t/(2t_0)} \Theta(t). \tag{3.7}$$

$E_{\rm s}(t)$ is displayed in the middle panel of figure 3. If a SR X-ray is scattered in succession by m resonant nuclei one obtains

$$E_{\rm s}(t) \propto \frac{(-{\rm i})^m t^{m-1}}{(m-1)!} {\rm e}^{{\rm i}\omega_0 t - t/(2t_0)} \Theta(t). \tag{3.8}$$

The drastic transformation of the wave packet by sequential nuclear scattering is seen in figure 3. It clearly shows that the re-emission of the γ-ray is more and more delayed with each next scattering event. This effect has recently been revealed as trapping of radiation by a nuclear ensemble [16]. In addition, figure 3 shows that the wave packet stretches noticeably over time with the number of scattering events (which corresponds, in accordance with the principle of uncertainty, to a sequential narrowing of the γ-ray energy distribution). This effect of stretching of the wave packet plays a crucial role in multiple nuclear forward scattering of a SR pulse in its propagation through a thick target (see sections 6.3 and 6.4). We also notice that by each scattering the phase of the wave packet is shifted by $-\pi/2$.

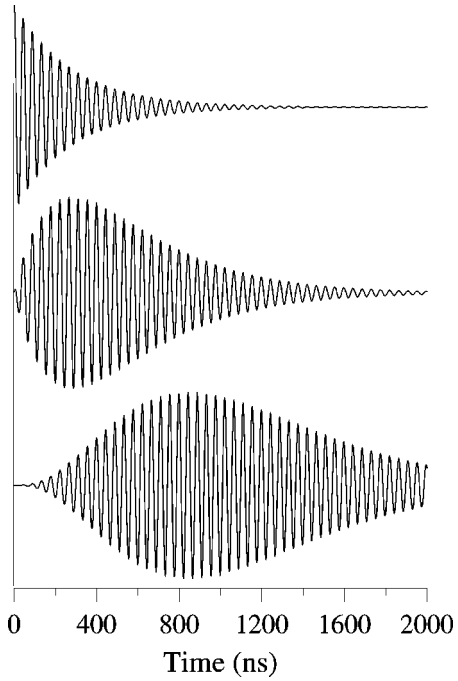

Figure 3. Time development of a SR X-ray wave packet due to sequential scattering by one, two and four nuclei (from the top).

The response function technique has been successfully used for finding the result of scattering from nuclear systems.

4. Elastic scattering from an ensemble of nuclei

4.1. The nuclear exciton

A γ-ray incident on an ensemble of identical nuclei can interact resonantly with each of them. The energy of the γ-quantum is only sufficient to excite a single nucleus in the ensemble. However, the observations of total reflection from a nuclear mirror and Bragg diffraction from a nuclear array in a crystal showed that not single nuclei but *nuclear ensembles are involved in scattering of single γ-quanta.*

These two seemingly contradictory facts were successfully combined in a physical picture, the notion of the delocalized nuclear excitation, which was introduced by Trammell [1] and by Kagan and Afanas'ev [2] (see also [13]).

In the case of elastic scattering of a γ-ray by a nuclear array, where the intrinsic state of the scattering system stays unchanged, it is impossible to ascertain which nucleus in the ensemble was excited. Therefore, accounting for the collective nuclear response, one may assume the possibility of excitation of each nucleus in accordance with the principle of superposition of states. In the superposition state the nuclear

excitation is delocalized and a γ-ray is thus shared by several nuclei. This is how the scattering process exhibits a collective character.

The experiments on total reflection and Bragg scattering revealed in addition the coherent nature of the delocalized excitation. The fact that wavelets re-emitted by nuclei interfere forming a diffraction pattern indicates a phase correlation of the constituent nuclear currents.

Thus the delocalized intermediate excited state created by a single γ-quantum can be understood as a spatially coherent superposition of excited states of all nuclei in the target. In each contributing term one nucleus is excited with a definite probability amplitude while all others are in the ground state. The spatial and temporal phasing of the excited nuclear currents over a system is determined by the space and time coherence of the field associated with the incident γ-ray. The superposition state of nuclear excitations is called a nuclear exciton. *The nuclear exciton has become a central concept of the theory of nuclear resonant scattering*. The nuclear ensemble behaves like a macroscopic resonator of which the properties differ qualitatively from those of individual nuclei. This is exhibited by changes of the time and space distribution of the nuclear decay products, in the redistribution of probabilities of the radiative and nonradiative channels of scattering, etc. In all these changes the coherence effects play a crucial role.

When the excitation is distributed over the entire nuclear ensemble and when the phase correlation of the partial nuclear excitations is preserved during the lifetime of the excited state, interference of the wavelets re-radiated by the nuclei occurs and a coherent radiation field is built up in nuclear resonant scattering.

4.2. Spatially coherent and incoherent scattering

While considering scattering of a γ-ray by a single nucleus in section 3 we were concerned with the correlation of the temporal part of the phase. In this subsection we concentrate our attention on the correlation of the spatial parts of the phases of the wavelets re-radiated by different nuclei in the nuclear ensemble.

Let us consider the scattering of a plane wave traveling in space with a propagation vector $\mathbf{k}_0$ by two nuclei, one of which is placed at the origin and the other at the site with coordinate $\mathbf{r}$. The amplitude of the wave scattered in the direction $\mathbf{k}_1$ is determined by interference of the wavelets scattered by the nuclei in this direction. It can easily be shown that the amplitude of the resulting wave is proportional to $1+\mathrm{e}^{\mathrm{i}\mathbf{s}\cdot\mathbf{r}}$, where $\mathbf{s}=\mathbf{k}_1-\mathbf{k}_0$ is called the scattering vector and the scalar product $\mathbf{sr}$ represents the difference between the spatial phases of the two wavelets. The total wave scattered by N nuclei in one direction is then given by the sum of the relevant N wavelets (so far we neglect multiple scattering)

$$E_{\mathrm{s}} \propto \sum_{a=1}^{N} \mathrm{e}^{\mathrm{i}\mathbf{s}\cdot\mathbf{r}_a}. \tag{4.1}$$

To find the wavefield intensity one must calculate the product E^*E, where E^* is the complex conjugate of E. This gives rise to a double sum in a and a'. In the product of two sums it is convenient to discuss separately the terms with $a = a'$, whose sum equals N, and those with $a \neq a'$:

$$E_{\rm s}^* E_{\rm s} = \text{const} \left\{ N + \sum_{a}^{N} \mathrm{e}^{-\mathrm{i}\mathbf{s}\cdot\mathbf{r}_a} \cdot \sum_{a' \neq a}^{N} \mathrm{e}^{\mathrm{i}\mathbf{s}\cdot\mathbf{r}_{a'}} \right\}. \tag{4.2}$$

The double sum accounts for the interference contributions from all pairs of atoms, a and a'. It is often called *pair correlation* function. When there is no spatial correlation in the atomic arrangement of the scattering system and $s \neq 0$ the relative phases $\mathbf{s}\cdot\mathbf{r}_a$ are homogeneously distributed over the interval 0–2π, so that the double sum in eq. (4.2) equals zero. Then the scattering intensity is simply proportional to the number of nuclei N. This is characteristic for *spatially incoherent scattering*, where the total scattering intensity is the sum of the intensities scattered by individual nuclei.

In the other special case, when the relative phase is zero or a multiple of 2π the summation in eq. (4.2) yields the product $N(N-1)$, so that the scattering intensity becomes proportional to the square of the number of nuclei N^2, typical for *spatially coherent scattering*. Fully constructive interference, as in our example, occurs in the case of an ordered arrangement of the ensemble of nuclei in all directions where the wavelets are in phase (entirely constructive Bragg reflection and forward scattering) or, in the case of disordered nuclei, only in the forward scattering direction, where $s = 0$.

The coherent constructive addition of the wavelets re-radiated by nuclei determines the physical nature of a *strong enhancement of the radiative channel of nuclear resonant scattering, the super-radiance effect* as given by Trammell [1] and Kagan and Afanas'ev [2] (see also Smirnov [13]). It is observed as a huge increase of the coherent scattering intensity, e.g., in Bragg diffraction from crystals, in total reflection from nuclear mirrors, and in forward scattering.

By contrast, destructive interference may lead to a vanishing amplitude of the scattered waves which results in *suppression of the elastic scattering channels, the sub-radiance effect* predicted by Kagan and Afanas'ev [2,17].

In the following sections we describe the main aspects of the dynamical theory of scattering which allows us to find the solutions for the coherent field of γ-radiation interacting with nuclear ensembles. For the original presentation of the theory see [12, 18–20] and references therein.

5. Aspects of the dynamical theory of γ-ray nuclear scattering

5.1. Maxwell equations for a space–time harmonic plane wave

The interaction of visible light and X-radiation with matter is analyzed with the help of the Maxwell equations. The Maxwell equations for a medium allow one to

find the solutions for the electric and magnetic fields due to the interaction of radiation with the medium. The Maxwell equations operate with the macroscopic polarization of the medium, accounting in this way for its response. The polarization represents the induced electric moment per unit volume.

The existence of a distributed coherent nuclear excitation, the nuclear exciton, provides the physical basis for the use of a macroscopic polarization given by the Maxwell equations to treat the radiative effects of nuclei. The macroscopic polarization of a nuclear ensemble is the sum of the induced nuclear transition moments over a unit volume, i.e., the density of the induced electric moment. It represents a quantum mechanical average over the nuclear ensemble.

For a medium without free charges the Maxwell equations can be used in the form

$$\nabla \times \mathbf{E} = -\frac{\partial \mathbf{B}}{\partial t}, \tag{5.1a}$$

$$\nabla \times \mathbf{H} = \frac{\partial \mathbf{D}}{\partial t}, \tag{5.1b}$$

where

$$\nabla = \mathbf{x}\frac{\partial}{\partial x} + \mathbf{y}\frac{\partial}{\partial y} + \mathbf{z}\frac{\partial}{\partial z}$$

is a differential operator with $\mathbf{x}, \mathbf{y}, \mathbf{z}$ unit vectors along the axes of a Cartesian coordinate system, $\mathbf{B}$ and $\mathbf{D}$ are the magnetic induction and the electric displacement vector, respectively. We assume that magnetically the scattering material has the same behaviour as empty space so that $\mathbf{B} = \mu_0\mathbf{H}$, where μ_0 is the magnetic permeability of empty space.

The electric displacement vector $\mathbf{D}$ is equal to the net effective polarization, which is the sum of the polarization induced by the electric field, $\mathbf{P}$, and the equivalent polarization due to the driving field $\mathbf{E}$. Regardless of the mechanism that gives rise to $\mathbf{P}$, it is always possible to express the induced polarization mathematically in a power series of $\mathbf{E}$. For many cases of interest, however, including our case, it is sufficient to retain only the term linear in $\mathbf{E}$:

$$\mathbf{P} = \varepsilon_0 \eta \mathbf{E}, \tag{5.2}$$

where ε_0 is the electric permittivity of empty space, which can also be regarded as a conversion factor that transforms the field $\mathbf{E}$ into an equivalent electric moment per unit volume, and η is the *electric susceptibility*. From the definition of the polarization of the medium as a sum of the induced nuclear transition moments per unit volume it is rather obvious that the susceptibility should be proportional to the coherent scattering amplitude f_c (particularly for forward scattering, where it is given by eq. (3.2)) and the number n of scattering centers per unit volume. The precise relationship is

$$\eta = \frac{\lambda^2}{\pi} n f_\mathrm{c}. \tag{5.3}$$

With

$$\mathbf{D} = \varepsilon_0 \mathbf{E} + \mathbf{P} \tag{5.4}$$

we obtain

$$\mathbf{D} = \varepsilon \varepsilon_0 \mathbf{E}, \tag{5.5}$$

where $\varepsilon = 1 + \eta$ is the dielectric constant of the material.

The total coherent field of γ-radiation in a medium can be decomposed into space and time harmonic plane waves (it refers to all field constituents: **E**, **B**, **D**). Equations (5.1) must be separately true for each individual elementary component of the coherent field.

$$\mathbf{E} = \mathbf{E}_0 \mathrm{e}^{\mathrm{i}(\omega t - \mathbf{k}\cdot\mathbf{r})}, \tag{5.6}$$

where **k** is the *wave vector inside the medium*. In general, it is a complex number. One immediately derives

$$\nabla \times \mathbf{E} = -\mathrm{i}\mathbf{k} \times \mathbf{E}_0 \mathrm{e}^{\mathrm{i}(\omega t - \mathbf{k}\cdot\mathbf{r})} = \mathrm{i}\mathbf{k} \times \mathbf{E} \tag{5.7}$$

and

$$\frac{\partial \mathbf{B}}{\partial t} = \mathrm{i}\omega \mu_0 \mathbf{H}. \tag{5.8}$$

Inserting eqs. (5.7) and (5.8) into eq. (5.1a) results in

$$\mathbf{k} \times \mathbf{E} = \omega \mu_0 \mathbf{H}. \tag{5.9}$$

The same procedure applied to eq. (5.1b), taking account of eq. (5.4), yields

$$-\mathrm{i}\mathbf{k} \times \mathbf{H} = \mathrm{i}\omega \varepsilon_0 \left(\mathbf{E} + \frac{1}{\varepsilon_0} \mathbf{P} \right). \tag{5.10}$$

Substituting **H** defined from eq. (5.9) into eq. (5.10) we obtain

$$\mathbf{k} \times (\mathbf{k} \times \mathbf{E}) = -K^2 \left(\mathbf{E} + \frac{1}{\varepsilon_0} \mathbf{P} \right), \tag{5.11}$$

where $K = \omega/c$ and $c = 1/\sqrt{\varepsilon_0 \mu_0}$. K is the magnitude of the wave vector and c is the velocity of light in vacuum. Making use of the vector identity $\mathbf{a} \times (\mathbf{b} \times \mathbf{c}) = -\mathbf{c}(\mathbf{a} \cdot \mathbf{b}) + \mathbf{b}(\mathbf{c} \cdot \mathbf{a})$ we finally obtain

$$\left(k^2 - K^2\right)\mathbf{E} - \mathbf{k}(\mathbf{k} \cdot \mathbf{E}) = K^2 \frac{1}{\varepsilon_0} \mathbf{P}, \tag{5.12}$$

which is the form of the *Maxwell wave equation for a space and time harmonic plane wave component of a γ-ray field in a medium*. In the approximation of eq. (5.2) one has

$$\left(k^2 - K^2\right)\mathbf{E} - \mathbf{k}(\mathbf{k} \cdot \mathbf{E}) = K^2 \eta \mathbf{E}. \tag{5.13}$$

Before proceeding to the solutions of this equation we make some general comments concerning fields in matter.

5.2. Dynamical wave equations

The radiation state can be radically transformed by interaction with matter. While propagating through matter radiation excites atomic currents which radiate their own waves, modifying the total field. When the re-emitted wavelets interfere constructively enhanced scattered waves are formed. The modification is especially strong if the target is thick enough to give rise to multiple scattering. The general scattering theory of visible light and X-rays developed by Ewald takes into account multiple scattering of radiation by atoms [21]. In the steady state a dynamic self-consistency is established between the radiation field and the induced currents: the total field created by the currents should be exactly that which creates those currents.

The total field represents a coherent superposition of the waves allowed by the scattering system. These waves are dynamically coupled via atomic currents feeding one another so that the total field must be considered as a single entity. Dynamic equilibrium between the field and the currents means that each constituent wave generates the whole set of eigenwaves and vice versa, each wave of the set contributes to the constituent wave. Let us consider the example of two eigenwaves allowed in a scattering system (illustrated schematically in figure 4). These could be, for instance, the waves propagating in the forward direction and having different polarization states or waves of the same polarization state propagating in forward and Bragg directions, respectively.

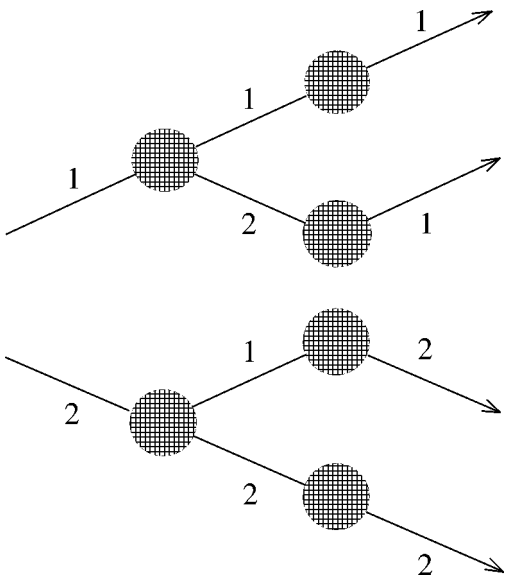

Figure 4. Coupling of two eigenwaves in a scattering system.

In figure 4 it is shown that wave 1 generates via induced currents the set of waves $1+2$. In turn, each wave of the set contributes to the formation of wave 1 and so on. The same transformation is true for wave 2. So the eigenwaves in this case can be connected in the set of Maxwell wave equations following from eq. (5.13):

$$\begin{aligned}\left(\frac{{k_1}^2}{K^2}-1\right)E_1 &= \eta_{11}E_1+\eta_{12}E_2,\\ \left(\frac{{k_2}^2}{K^2}-1\right)E_2 &= \eta_{21}E_1+\eta_{22}E_2.\end{aligned} \tag{5.14}$$

Equations (5.14), originating from the condition of dynamic equilibrium, are often referred to as dynamical wave equations. The parameters $\eta_{\alpha\beta}$ are the amplitudes of Fourier components of a relevant Fourier expansion of the electric susceptibility of the scattering medium. We shall refer to them as the susceptibility amplitudes. They form a scattering matrix each term of which is related to the propability amplitude of the transition from the eigenstate β of the radiation field to the eigenstate α. In the present case the matrix is of second rank. In writing down eqs. (5.14) we have assumed that the electromagnetic field inside a target is practically transverse, i.e., $\mathbf{E}\cdot\mathbf{k}=0$.

The nuclear array in a crystal in the presence of a hyperfine interaction represents an optically active and diffracting medium. Therefore, in general the eigenwaves can be of different polarization states and can have different propagation vectors, related by the Bragg conditions. The Maxwell wave equation (5.13) then splits into a *set of dynamical wave equations*, connecting each constituent wave with all others,

$$\left(\frac{k_d^2}{K^2}-1\right)E_d^{\xi}=\sum_{d',\xi'}\eta_{dd'}^{\xi\xi'}\,E_{d'}^{\xi'}, \tag{5.15}$$

where the index d denotes the propagation directions and the index ξ labels the projection of the $\mathbf{E}_d$-vector on the ξ-axis of the coordinate system (for Cartesian coordinates $\xi=x,y,z$). Usually the basis of mutually orthogonal unit vectors $\mathbf{e}^{\pi}$ and $\mathbf{e}^{\sigma}$ (conventionally oriented with respect to the scattering plane) is used to describe an arbitrary polarization state of the radiation. By making use of this basis the set of dynamical equations can be reduced.

The explicit form of the susceptibility amplitudes $\eta_{dd'}^{ss'}$ must be derived for each particular scattering problem using the chosen polarization basis. The *set of the dynamical equations together with the boundary conditions is sufficient for finding the propagation vectors, the polarization states and the scalar amplitudes of the constituent eigenwaves*. We note that the magnitude of a propagation vector in matter is only slightly different from that in empty space because of the weak interaction of γ-radiation with matter.

In a disordered and optically isotropic medium only a single coherent wave is generated in the forward direction. *The susceptibility in this case is a complex scalar* η (eq. (6.4)). The main effect of the medium is a phase shift and an attenuation of the amplitudes of the transmitted wave.

In a disordered but optically anisotropic and active medium waves of different polarization states propagating in the forward direction can be excited (section 6.8). The susceptibility amplitudes then form a matrix of second rank $\eta^{ss'}$, where s and s' mean either σ or π. The optical activity of the nuclear system arises from the hyperfine splitting of the nuclear transitions. A wealth of polarization phenomena in transmission of γ-rays through the nuclear target can be observed, such as birefringence: dichroism, double refraction, and optical activity: the Faraday effect (eq. (6.27)).

In an ordered nuclear array diffraction phenomena can occur. In the case of a single Bragg reflection two directions are permitted for coherent scattering. In the absence of optical activity the susceptibility amplitudes again form a (2×2) matrix $\eta_{dd'}$, where the indices d, d' denote the forward and the Bragg reflection directions. Bloch waves of radiation are then formed which have both running and standing wave behaviour. Thereby the standing wave periodicity matches that of the crystal. For this reason the Bloch waves exhibit anomalous interaction with the scattering centers, having, in particular, anomalously weak or strong absorption by atoms (Borrmann effect in the case of interaction with electronic shells, Kagan–Afanas'ev effect in the case of nuclear interaction).

In the presence of optical activity in the diffracting medium the susceptibility amplitudes in general form a (4×4) matrix $\eta_{dd'}^{ss'}$ [18].

In this paper we limit ourselves to the analysis of the particular cases of nuclear resonant scattering of SR in the forward direction.

6. Nuclear forward scattering

6.1. Transmission of a wave in an optically isotropic medium

For the most frequently used disordered atomic system the forward direction is a particular one because the only scattered waves contributing in phase are those which propagate in the same direction as the incident beam. In such disordered systems spatially coherent scattering of γ-rays exists only in this direction. The coherently scattered wave modifies the incident wave, yielding the transmitted wave. Thus, the *propagation of a wave in the forward direction is a coherent process*.

We assume the medium to be optically isotropic. In such media scattering is not sensitive to the polarization state of the radiation, in other words the susceptibility is represented by a scalar number. Therefore, the solution for the coherent field in the medium can be given as a single arbitrary polarized wave propagating in the direction of incidence. The set of dynamical equations is reduced to a single equation for the scalar amplitude of the wave:

$$\left(\frac{k^2}{K^2} - 1\right) E = \eta_0 E. \tag{6.1}$$

We choose the geometry given in figure 5: the sample is a plane parallel plate put perpendicular to the z-axis. The entrance surface of the plate is at $z = 0$. The direction

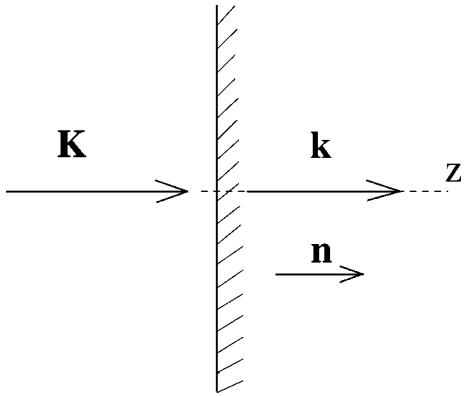

Figure 5. Wave propagation geometry.

of incidence is along the $+z$-axis, $\mathbf{n}$ is a unit vector directed along the inward surface normal. The incident wave is $E_i = E_0 \mathrm{e}^{\mathrm{i}(\omega t - Kz)}$.

Inside the target the propagation vector is

$$\mathbf{k} = \mathbf{K} + \delta K \mathbf{n}, \tag{6.2}$$

where δ is a small complex number accounting both for absorption and refraction of the medium. By definition the sum $1 + \delta$ is the index of refraction of the medium. Substituting eq. (6.2) into eq. (6.1) and neglecting terms of second order we find

$$\delta = \frac{1}{2}\eta_0. \tag{6.3}$$

The nuclear susceptibility is obtained from eqs. (5.3) and (3.2)[2]:

$$\eta_0 = -\frac{1}{K}\mu \frac{\Gamma/2\hbar}{\omega - \omega_0 - \mathrm{i}q\Gamma/2\hbar} \quad \text{with} \quad \mu = \sigma_0 f_{\mathrm{LM}} \beta n, \tag{6.4}$$

where μ is the linear absorption coefficient at resonance (the parameters involved are defined in eqs. (3.2) and (5.3)). In addition, we have inserted a factor q describing a broadening of the resonance, which preserves, however, the Lorentzian shape, $q\Gamma = (1 + \Delta)\Gamma$ [13].

Obviously, the nuclear susceptibility has the same frequency dependence as the scattering amplitude, see figure 1. Taking into account the boundary condition, $E = E_0$, we obtain for the transmitted wave

$$E_{\mathrm{tr}} = E_0 \mathrm{e}^{\mathrm{i}\omega t - \mathrm{i}K(1+(1/2)\eta_0)z} = E_i \mathrm{e}^{-\mathrm{i}(1/2)\eta_0 K z} \tag{6.5}$$

and for the transmitted intensity

$$I_{\mathrm{tr}} = I_0 \mathrm{e}^{K\mathrm{Im}(\eta_0)z} = I_0 \mathrm{e}^{-\mu z/(\Delta^2+q^2)}, \tag{6.6}$$

[2] The electronic susceptibility should be added to the nuclear one to get the total susceptibility. In the resonance range it is a constant which we did not take into account so far.

where $\Delta = \hbar(\omega - \omega_0)/(\Gamma/2)$ is the deviation from resonance in units of the half width of the nuclear level. It is seen from eqs. (6.5) and (6.6) that the attenuation of the wave amplitude and the absorption of γ-radiation in a nuclear target, respectively, are determined by the imaginary part of the nuclear susceptibility. The real part of the susceptibility gives rise to a phase shift of the transmitted wave with respect to the incident one, which, however, is not detected in a standard transmission measurement but can be important in a coherent scattering measurement. From the frequency dependences of the imaginary and real parts of the susceptibility (which are like those displayed in figure 1(c)) it is immediately seen that at exact resonance the absorption is strongest and no phase shift takes place, whereas in the wings of the resonance the absorption is weak and can be accompanied by a large phase shift depending on the thickness of the target.

It is instructive to consider the field transmitted through a thin layer Δz with $\eta_0 K \Delta z \ll 1$. Expansion of $E_{\rm tr}$ in eq. (6.5) yields

$$E_{\rm tr}(\omega) \approx E_{\rm i}\left[1 - {\rm i}\frac{1}{2}\eta_0(\omega)K\Delta z\right]. \tag{6.7}$$

The first term in eq. (6.7) represents the incident wave, as for the second one, it turns out to be equal to the wave scattered by the layer in the forward direction, $E_{\rm fs}$, as obtained in the direct summing of the wavelets coherently re-radiated by the nuclei in the layer to the point of observation. The phase shift due to the scattering by a plane target is $-\pi/2$ ($e^{-i\pi/2} = -i$) as a result of the interference of the wavelets arriving from the plane target area. Equation (6.7) shows in which way the scattered wave modifies the incident wave. Particularly, at resonance, where an additional phase shift of $-\pi/2$ appears (see figure 1(b)) the forward scattered wave is in antiphase with the incident wave, yielding the strongest attenuation of the transmitted wave amplitude and hence the drop in transmitted intensity. The destructive interference between the incident and forward scattered waves gives rise to 4π scattering of γ-radiation and conversion electron emission.

Equation (6.7) represents the first iteration in building up the transmitted field.

In general, one can say that two independent paths occur with well defined probabilities of transmission of a γ-ray through a target of arbitrary thickness, namely: transmission without interaction, and coherent forward scattering by the target. In such a presentation the wavefield transmitted through the target is a coherent superposition of the incident and the forward scattered waves (coherence between the emission of the γ-ray by the source and its re-emission by the target is assumed):

$$E_{\rm tr} = E_{\rm i} + E_{\rm fs}. \tag{6.8}$$

The reality of the forward scattered wave in the presence of primary radiation can be demonstrated in experiments where conditions are provided to either observe the interference between the frequency components of the transmitted radiation or to control the interference between the primary (incident) and the secondary (forward scattered) waves. These are experiments with a conventional Mössbauer source where the prop-

agation of a γ-ray through a resonant absorber is observed, e.g., as a function of time, with the help of the delayed coincidence technique [22]. Another way to reveal forward scattering is to apply amplitude modulation of the incident beam, the shutter technique ([6] and references therein), or phase modulation of the incident or scattered radiation (see, e.g., [23–25]).

The new SR sources provide an excellent opportunity to observe pure forward scattering because with these sources the incident and the forward scattered wave trains are perfectly separated in time. Thus in the experiments with a SR source we may consider the forward scattered radiation separately rather than coupled intrinsically with the incident radiation as in experiments with a Mössbauer source.

Concluding this subsection we write down the expressions for a frequency component of the forward scattered radiation for a thin layer (where the coupling of nuclei with the scattered radiation is neglected)

$$E_{\mathrm{fs}}^{l}(\omega) \approx -\mathrm{i}\frac{1}{2}E_i\eta_0(\omega)K\Delta z \tag{6.9}$$

and for a target of arbitrary thickness

$$E_{\mathrm{fs}}(\omega) = E_{\mathrm{i}}\left(\mathrm{e}^{-\mathrm{i}(1/2)\eta_0(\omega)Kz} - 1\right). \tag{6.10}$$

(In the latter case the coupling of the secondary radiation with nuclei is taken into account.)

6.2. Time response of nuclear target, speed-up, dynamical beat

In section 3.3 we have described the transformation from the energy to the time domain while regarding the scattering of a γ-ray by an isolated nucleus. Using the same approach we now describe the transmission of a SR X-ray through a resonant absorber in time. The wave packet transmitted through a thin layer can be obtained by integrating all components $E_{\mathrm{tr}}(\omega)$ given by eq. (6.7):

$$E_{\mathrm{tr}}(t) = \varepsilon_{\omega_0}\frac{1}{2\pi}\int_{-\infty}^{\infty}\mathrm{d}\omega\left[1 - \mathrm{i}\frac{K}{2}\eta_0\Delta z\right]\mathrm{e}^{\mathrm{i}\omega t}, \tag{6.11}$$

where the frequency component of the incident synchrotron radiation is $\varepsilon_{\omega_0}\mathrm{e}^{\mathrm{i}\omega t}$ (see section 2.2). The first integral in eq. (6.11) yields the δ-function. The second integral can be evaluated as described in section 3.3. Substituting eq. (6.4) into eq. (6.11) we finally obtain the time response of a thin layer to a δ-function-like excitation

$$E_{\mathrm{tr}}(t) \approx \varepsilon_{\omega_0}\left[\delta(t) - \frac{1}{4t_0}\mu\Delta z\mathrm{e}^{\mathrm{i}\omega_0 t - t/(2t_0)}\right], \quad t \geqslant 0. \tag{6.12}$$

The transmitted packet consists of the prompt contribution at time zero by the incident radiation and of an exponentially decaying part representing the delayed forward scattered radiation. The expression in the square brackets is *the time response function of a thin plane layer*. The response is obtained in the kinematical approximation where the

interaction with the primary radiation only is taken into account. The exact solution, which follows, takes into account the coupling of nuclear currents with both primary and secondary radiation.

The wave packet at an arbitrary depth z in the target is obtained by integrating the frequency components eq. (6.5). Performing the integration we arrive at an expression for the wave packet similar to that obtained in [26]:

$$\begin{aligned} E_{\rm tr}(z,t) &= \varepsilon_{\omega_0} {\rm e}^{-\frac{\mu_e z}{2}} \left[\delta(t) - \frac{1}{2t_0} \mu z {\rm e}^{{\rm i}\omega_0 t - qt/(2t_0)} \sigma(z,t) \right], \\ \sigma(z,t) &= \frac{{\rm J}_1(\sqrt{\mu z t/t_0}}{\sqrt{\mu z t/t_0}}, \quad t \geqslant 0, \end{aligned} \tag{6.13}$$

and for the forward scattering intensity (taking into account eq. (2.5))

$$I_{\rm fs}(z,t) = I_0 \frac{\Gamma}{\Delta E} \cdot {\rm e}^{-\mu_e z} \cdot \frac{(\mu z)^2}{4t_0} \cdot {\rm e}^{-qt/t_0} \sigma^2(z,t), \tag{6.14}$$

where the photo-electronic absorption in the target is taken into account: μ_e is the relevant absorption length, I_0 is the stationary intensity of the SR within the energy band ΔE determined by a monochromator and $\rm J_1$ is the Bessel function of first order.

The space–time structure of the forward scattered wave packet is represented by the second term of eq. (6.13). We note that the function σ entering in eq. (6.13) is a function of a generalized coordinate, namely of a product of space and time coordinates. This result is closely related to the space–time periodicity of the radiation wavefield which contains both temporal and spatial phases. It is convenient to use dimensionless coordinates of space and time: effective thickness $T = \mu z$ and reduced time $\tau = t/t_0$. The value of the function σ at the point $T\tau = 0$ is $1/2$. Thus, for $T\tau \ll 1$ the time dependence given by eq. (6.13) approaches that of eq. (6.12) at $q = 1$.

We consider the initial stage of the decay. The duration of the initial stage can be determined by the condition $T\tau \approx 3$. Within the time window $\tau = 3/T$ the function σ can be approximated by an exponential $\sigma(T\tau) \approx (1/2)\exp(-T\tau/8)$ so that we get for the forward scattered wave packet

$$E_{\rm fs} \propto T {\rm e}^{-(\tau/2)(q+T/4)} \quad \text{and for the intensity} \quad I_{\rm fs} \propto T^2 {\rm e}^{-\tau(q+(T/4))}. \tag{6.15}$$

The features of super-radiance specific for coherent nuclear scattering are immediately seen at the initial stage of the decay. First of all, it is an enhanced scattering intensity, which is proportional to T^2, i.e., $\sim (nz)^2$, the square of the number of nuclei on the beam path in the target per $\rm cm^2$. This enhancement is caused by the collective coherent response of all nuclei in the scattering ensemble which leads to constructive interference of the scattering paths via separate nuclei. As a result, the probability of radiative decay in the forward direction increases drastically. This effect already arises in the kinematical approximation of the scattering theory where only coupling of the nuclei with the incident radiation is accounted for.

The next feature is a speeding up of the nuclear decay determined by the exponential index $T/4$, i.e., by the effective thickness of the nuclear target. This effect appears when one also takes into account the coupling of nuclei with the secondary, coherently scattered radiation. Obviously, the effect of coupling gets stronger with the amplitude of the coherent field, i.e., with the increase of the depth in the nuclear target. The nuclei at a depth excited initially by the prompt part of the propagating wave packet eq. (6.13) are then exposed to the delayed part of the packet. So one could say that they perform a driven kind of decay similar to stimulated emission and in that sense the speed-up effect has similarities with the stimulated emission. However, one should remember that in our case we treat a single photon scattering event and in fact have to deal with the coherent superposition of different scattering channels rather than with the real stimulated emission.

As seen from eq. (6.15) there is another reason for accelerated coherent emission. It is related to the broadening of the resonance introduced by the factor q (see eq. (6.4)). However in contrast to the speed-up effect, which manifests the enhancement of the radiative channel, this acceleration reveals the breakdown of the coherent signal due to inhomogeneous resonance broadening. This broadening is accompanied by a loss of intensity in the coherent channel and a re-distribution of the scattered intensity in favour of the incoherent channel [27]. We illustrate the effect of resonance broadening in section 6.7.

The time integral scattering intensity is approximately proportional to T^2, however, only for a thin target, $T < 1$. The thickness dependence of the time integral nuclear forward scattering intensity, $I_{\rm int}(T) \propto {\rm e}^{-\mu_e z} \int_0^\infty {\rm d}\tau \cdot {\rm e}^{-q\tau} \sigma^2(T\tau)$, is depicted in figure 6. It is calculated for the case of a fully enriched stainless steel target (no broadening of the resonance is assumed) taking into account the electronic absorption $\mu_e z$ by the target material: $\mu_e \approx 0.05\ \mu{\rm m}^{-1}$.

The electronic absorption causes an exponential decrease of the intensity with an increase of thickness, in this way limiting the number of nuclei which participate in the coherent scattering. Yet in the range of thin targets its influence is low: in the top panel of figure 6 the intensity rises in between the first and second power of the thickness parameter T. Then due to the electronic absorption the increase of intensity slows down, the forward scattering intensity reaches a maximum and starts to decrease (bottom panel of figure 6). Finally, the electronic absorption becomes dominant and the intensity drops to zero.

We turn back to the analysis of the space–time structure of the FS wave packet and now consider the limit of large times and thick targets. There the function σ determines the modulation of the propagating wave packet both in time – as observed at the point of observation, and in space – as observed at fixed time. This function has zeros at values 14.8, 49.2, ... of its argument $T\tau$ giving rise to a *node–antinode structure of the wave packet*, see figure 7. At the node regions the oscillation at the carrier frequency drops to zero, in passing the node points the oscillation grows again but its phase gets inverted due to changing the sign of the function σ (compare the phasing of the oscillation around the node points O_1 and O_2 in figure 7). The

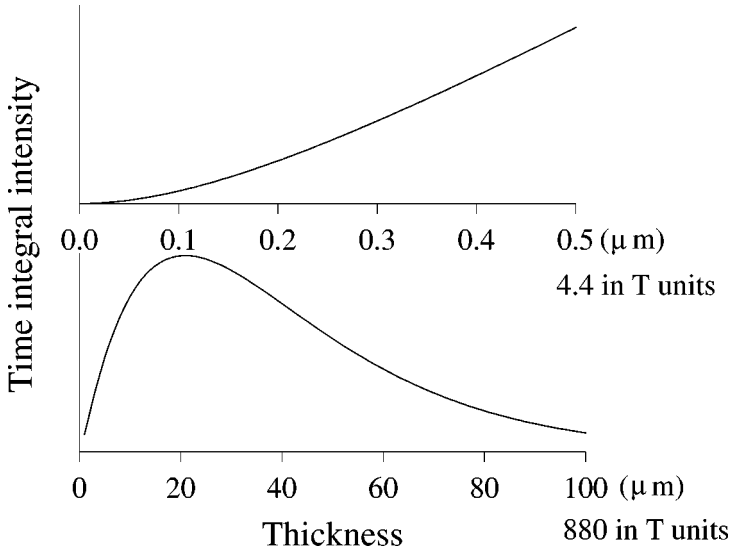

Figure 6. Time integral intensity of forward scattered synchrotron radiation as a function of the thickness of a nuclear target – ^{57}SS foil.

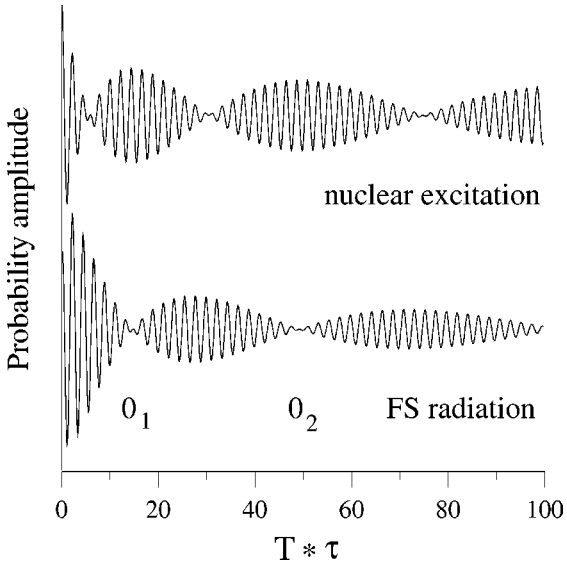

Figure 7. Node–antinode structure of the probability waves of the nuclear excitation and of the coherent radiation field.

pronounced node–antinode structure of the wave packet is a dramatic consequence of the propagation of a γ-ray through a thick resonant target. The modulation of the scattering intensity in time and in space is called *propagation* or *dynamical beat*. The relevant space–time pattern can be imagined as a train of zones of “brightness” and

"darkness" traveling in space along the propagation direction. The zones' width is stretching at later times. In the next subsection we briefly discuss the physical nature of dynamical beats.

6.3. Coupling of the radiation field and nuclear currents, multiple scattering

Each atom excited by the coherent field propagating through the target becomes a source of secondary radiation. Along with the directed coherent beam of γ-radiation the 4π shine of γ-rays, conversion electrons, and fluorescent X-rays appears around a target due to *spatially incoherent scattering of the propagating wave* (section 4.2). The incoherent emission of nuclei detected at a definite depth in the target demonstrates the nuclear excitation state at this depth. Let us find the wave packet of a γ-ray re-emitted into 4π by a nucleus situated at depth z. In the process of nuclear resonant scattering of SR two channels should be distinguished: nuclear excitation with and without recoil [27–29] (see also section 6.7). Here we limit ourselves by regarding only the recoilless radiative channel of scattering. The amplitude of the wavelet re-emitted by a bound nucleus at depth z can be found by employing the response function technique (section 3.4):

$$E_{4\pi}(z,t) = \int_{-\infty}^{\infty} \mathrm{d}t' \cdot f_{\mathrm{c}}\big(t-t'\big)\, E_{\mathrm{tr}}\big(z,t'\big), \tag{6.16}$$

where E_{tr} represents the wave packet of the propagating coherent γ-radiation at the nuclear site and f_{c} is the response function of the nucleus with a time dependence identical with that given by eq. (3.5). We substitute eqs. (6.13) and eq. (3.5) into eq. (6.16). Then we perform the integration using

$$\frac{\partial \mathrm{J}_0(\sqrt{T\tau})}{\partial t} = -\frac{T}{2t_0}\frac{\mathrm{J}_1(\sqrt{T\tau})}{\sqrt{T\tau}}$$

and obtain

$$E_{4\pi}(T,\tau) \propto \mathrm{e}^{\mathrm{i}\omega_0 t - \tau/2}\mathrm{J}_0(\sqrt{T\tau}), \tag{6.17}$$

where J_0 is the Bessel function of zero order. First of all we see that the time response of the nuclei at the surface of a target ($z = 0$) coincides with the free response of a single nucleus eq. (3.5) (since $\mathrm{J}_0(0) = 1$), which is simply an exponential decay. This result is quite evident because these nuclei are illuminated only by the pulsed synchrotron radiation. However, at finite depth in the target a nucleus is illuminated initially by the SR pulse (the prompt constituent of the propagating wave packet) and then by the delayed γ-radiation which is forward scattered by the upstream part of the target. It now responds as a driven oscillator. The time response of this nucleus is modified by the function J_0, i.e., it is first accelerated and then strongly modulated in time.

In figure 7 the wave packet re-emitted in 4π by a single nucleus is compared with the coherent field at the depth of location of the nucleus. As seen from the

figure the incoherent response of a nucleus exhibits a node–antinode structure as well, which, however, is shifted with respect to that of the propagating field. The maxima of incoherent emission are reached at time–space coordinates where the amplitude of the propagating field drops to zero.

Remembering that 4π scattering reveals the nuclear excitation we can say that the nuclear excitation in the target is also modulated both in time and in space. The node–antinode pattern of the excitation amplitude is strongly related to that of the coherent field as seen from figure 7. Both are traveling along the propagation direction. The complete disappearance of the γ-quantum in the propagating field at the points O_1 and O_2 coincides with the maximal probability amplitude of nuclear excitation and, on the other hand, a zero excitation amplitude coincides with the largest probability to find a quantum in the propagating field. This picture reflects the dynamics of "pumping" the electromagnetic energy from the radiation field to the nuclear system and back while a γ-ray propagates in the resonant medium. It is known from classical optics that in *transient* phenomena a relationship between the phase of the driving field and the driven dipole moment determines the direction of the energy transfer. It is quite obvious that at the node points where the relative phase between radiation and nuclear dipoles is inverted (shifted by π) the transition between the regimes of emission and absorption of γ-rays by nuclei occurs. Thus the *space–time modulation of both the nuclear excitations and the propagating field reveals sequential absorptions and re-emissions of radiation by nuclei. The number of antinodes in the radiation wave packet shows the number of scattering events in the observation window for a given target.* Multiple scattering occurs in thick targets and becomes apparent only after some time of interaction of γ-radiation with the nuclear ensemble.

The time gap between the sequential scattering events is related to the lifetime of the intermediate excited state, in other words to the collision time. It can be shorter than the natural lifetime because of the collective coherent action of the nuclear ensemble leading to the speed-up effect. The energy exchange between the radiation field and the nuclear currents gradually slows down (the collision time increases) as seen in figure 7: compare the intervals between nodal points. This slowing down of the energy exchange has to do with the stretching of the γ-ray wave packet in time after each following collision (see figure 3). With each following scattering event the energy distribution is getting narrower and hence is more and more localized at the resonance. The closer to the resonance energy the excitation occurs the longer the intermediate excited state lives (see, e.g., [30]). We turn again to the nature of the aperiodicity in the next subsection.

At the first instant after passage of the SR pulse through the target all nuclear currents are excited with equal probability amplitude. Later a node–antinode structure is built up in the target with nodal planes moving towards its front surface as a function of time fulfilling the condition of the nodal plane position $T\tau = \text{const}$. It is of interest to estimate the velocity of moving the antinode planes of nuclear excitation in the target. Let us consider the node at $T\tau = 14.8$. At depth $T_1 = 100$, for example, it will appear at $\tau_1 = 0.148$, while at depth $T_2 = 50$ it will arrive at $\tau_2 = 0.296$. The

nodal plane is moving in the direction from the back to the front of the target. This is quite natural because the secondary γ-ray–nuclear interaction first occurs deeper in the target. The motion proceeds with the average reduced speed $\bar{\nu} = (T_1 - T_2)/(\tau_1 - \tau_2)$. If the target material consists of SS made with pure ^{57}Fe, where $\mu \approx 8.8$ μm^{-1} and $t_0 \approx 141$ ns, we obtain $\bar{\nu}/\mu t_0 \cong 3 \cdot 10^4$ cms^{-1}, which is surprisingly small.

Thus, in accordance with the statement made before, the nuclear exciton represents a coupled system of the γ-ray field and the nuclear excitations. The development of the nuclear exciton in space and time is illustrated by the above description.

6.4. The double-hump profile of forward scattered radiation

The role of multiple scattering in the formation of dynamical beats is revealed by considering the scattering event in the time domain. It is also helpful to find the physical reason for the dynamical beats using the frequency or energy domain. We turn back to the solution for the scattered field in the energy domain eq. (6.10) and plot the square of the oscillation amplitudes as a function of energy. These spectra of the forward scattered radiation are depicted in figure 8 (middle column) for the cases of thin and thick targets. The Mössbauer transmission spectra for the same targets are shown for comparison in the left column. A dramatic change in shape of the scattering spectra is observed, in contrast to the moderate change of the shape of Mössbauer transmission spectra.

In the Mössbauer spectra the lineshape stays qualitatively the same with thickness. As to the scattering spectrum, it has a simple Lorentzian shape for a thin target whereas for a thick one, a 3 μm thick ^{57}SS foil, it develops a pronounced *double-hump profile*.

Such a double-hump profile can be understood on the basis of the relationship given by eq. (6.8), the geometrical image of which in the complex plane is shown in figure 9 for a 3 μm thick ^{57}SS target. All frequency components of SR have the same amplitude denoted as E_i (see eq. (2.5)). The amplitude $E_{\rm tr}(\omega)$ and the phase $\alpha(\omega)$ of a transmitted frequency component are determined by the deviation $\omega - \omega_0$ from resonance. The blank dot in figure 9 corresponds to infinite deviation and the bold dot indicates the resonance position. The phase and amplitude relationship between the incident and transmitted components determines the scattered component. The three relevant arrows form a triangle in the complex plane. While moving towards resonance from $-\infty$ one corner of the triangle glides along the solid curve through sequential points 1, 2, 3. One can easily follow the amplitude of the forward scattered spectral component $E_{\rm fs}$ developing in this motion. At a large deviation from resonance the transmitted wave is close to the incident wave both in amplitude and phase (vicinity of the blank dot). In this limit the FS wave has a vanishing amplitude, $|E_{\rm fs}| \approx 0$. Near resonance, where the real part of the nuclear scattering amplitude dominates over the imaginary part (somewhere about $\pm 10\Gamma$ off resonance, see figure 1(c)), the transmitted wave is still attenuated a little but its phase is changed drastically, see point 3. In this range $|E_{\rm fs}| \approx |2E_i|$. At exact resonance the transmitted wave is strongly attenuated in a thick target (vicinity of the bold dot). This is because

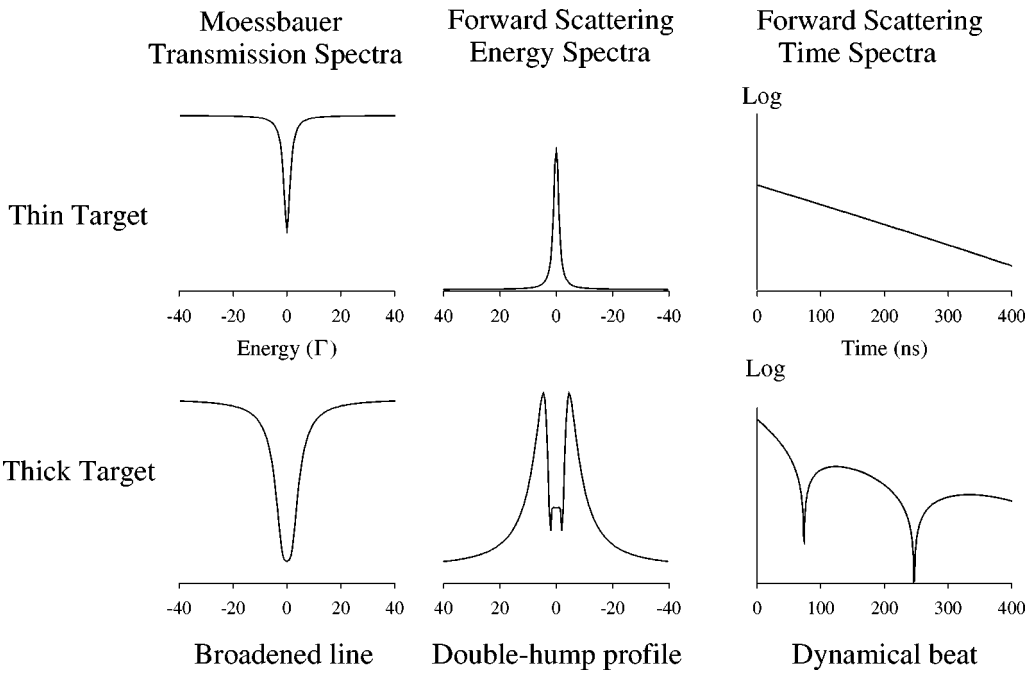

Figure 8. Mössbauer transmission spectra – left column, and synchrotron radiation scattering spectra in energy and time domain – middle and right columns, respectively, for the case of a single resonance in a thin target (0.2 μm thick ^{57}SS foil) – upper panel, and in a thick target (3 μm thick ^{57}SS foil) – lower panel.

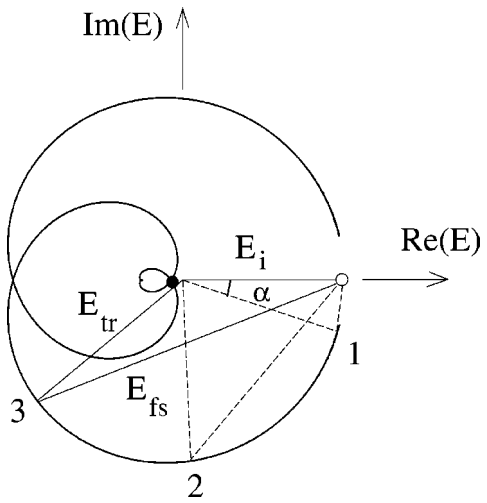

Figure 9. Relation between incident, forward scattered and transmitted fields in steady state eq. (6.8) in the complex plane for a 3 μm thick ^{57}SS foil. The blank dot is at infinite deviation of the energy from resonance, the bold dot is at the exact resonance energy. The phase α between E_i and $E_{\rm tr}$ is increasing towards the resonance.

of destructive addition of incident and FS waves which are of about the same amplitude $|E_{\rm fs}| \approx |E_i|$ at this point but in opposite phases. The same evolution occurs in the frequency range above resonance and in this way the double-hump structure results. It follows from the discussion that such a profile develops due to propagation of white radiation in a thick layer of a resonant medium. In fact several humps can result in approaching the resonance in a thick target but the outermost humps are most pronounced.

According to our interference picture the time modulation of the propagating packet can be interpreted as a beat between the two pronounced groups of radiation components distributed symmetrically to the left and right of the resonance frequency. Since these two groups are formed in scattering by a single resonance one can understand the dynamical beats as a result of *intra-resonance interference*. The beat frequency is determined by the separation of the maxima. Both the distance between the maxima and the beat frequency grow as the target thickness increases. The considered double-hump structure of the FS spectrum of SR is characteristic for the steady state picture of scattering. Such a frequency distribution is obtained by integration of the delayed part of eq. (6.13) over the full time range $0 \leqslant t < \infty$. It is instructive to trace the evolution of the shape of the FS energy spectrum with the increase of time after excitation. The spectra formed in an extending time window are shown in figure 10 for the time windows 0–20 ÷ 0–200 ns in the case of a 3 μm thick ^{57}SS target. The formation and development of the double-hump structure of the spectrum is clearly seen in the figure. In the initial stage the radiation components form a spectrum of very large width. Somewhat later their distribution is getting narrow and growing at resonance. However, at about 80 ns two humps start rising at the sides of the resonance which at later times become very pronounced. The separation of the humps gradually decreases with time.

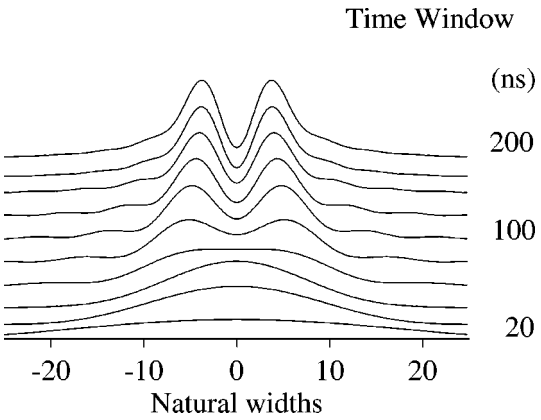

Figure 10. Formation and development of a double-hump profile of the spectrum of SR scattered in the forward direction by nuclei in a 3 μm thick ^{57}SS foil with increasing observation time after excitation of the nuclear ensemble. The appearance of humps at about 80 ns observation time coincides with the occurrence of the first beat minimum in the time spectrum in figure 8.

The described features of the FS spectrum correlate well with the main features of the time dependence in figure 8: the broad frequency distribution corresponds to the very fast initial decay and hence to a short collision time at this stage; the occurrence of two humps coincides with the beginning of beating; the decrease of the distance between the humps corresponds to the increase of the beat period with time (see figure 8). The properties of γ-ray pulse propagation through resonant media are extensively compared with those in the infrared and the visible in the case of molecular, atomic and excitonic resonances in [31].

Let us now consider the effect of splitting of the resonance on the evolution of nuclear forward scattering.

6.5. Resonance splitting, quantum beat

It is a frequently encountered situation in Mössbauer spectroscopy that nuclear levels are shifted at different nuclei or split due to hyperfine interaction. The electric monopole, electric quadrupole and magnetic dipole hyperfine interactions are of particular importance. The nuclear susceptibility then splits into several terms with different transition frequencies

$$\eta_0(\omega) = \text{const} \sum_j \alpha_j R(\omega - \omega_j) \quad \text{with} \quad R(\omega - \omega_j) = \frac{\Gamma/2\hbar}{\omega - \omega_j - \mathrm{i}\Gamma/2\hbar}, \tag{6.18}$$

where α_j is the strength of a particular resonance transition. When $2\hbar \cdot |\omega_{j'} - \omega_{j''}| \gg \Gamma$ the spectrum of FS radiation contains distinctly resolved frequency components. The interference between the resolved components, *inter-resonance interference*, yields a beat pattern termed *quantum beat* [32,33]. For simplicity we limit our discussion by considering forward scattering from a thin plane layer with nuclei having two resonances. Two terms appear in eq. (6.9) in this case and the spectrum of FS radiation is presented by two groups of oscillators of equal strength as shown in figure 11 upper panel.

Substituting eq. (6.18) into eq. (6.9) and executing the integration (as described in section 3.3) we obtain the solution for the FS scattered wave packet

$$E_{\text{fs}}(t) = \text{const} \sum_{j=1,2} \alpha_j \mathrm{e}^{\mathrm{i}\omega_j t - t/(2t_0)} \tag{6.19}$$

and for the FS intensity ($\alpha_1 = \alpha_2$)

$$I_{\text{fs}}(t) = \text{const} \cdot \mathrm{e}^{-t/t_0} \big\{ 1 + \cos(\omega_1 - \omega_2)t \big\}. \tag{6.20}$$

The overall time dependence characteristic for the decay of a nuclear state with a Lorentzian energy distribution is still observed, however, it is strongly modulated due to interference between the resonance components of eq. (6.19). The quantum beat pattern of the time spectrum is depicted in figure 11 upper right. The quantum beat of the scattering intensity demonstrates that the decay of the nuclear exciton in the

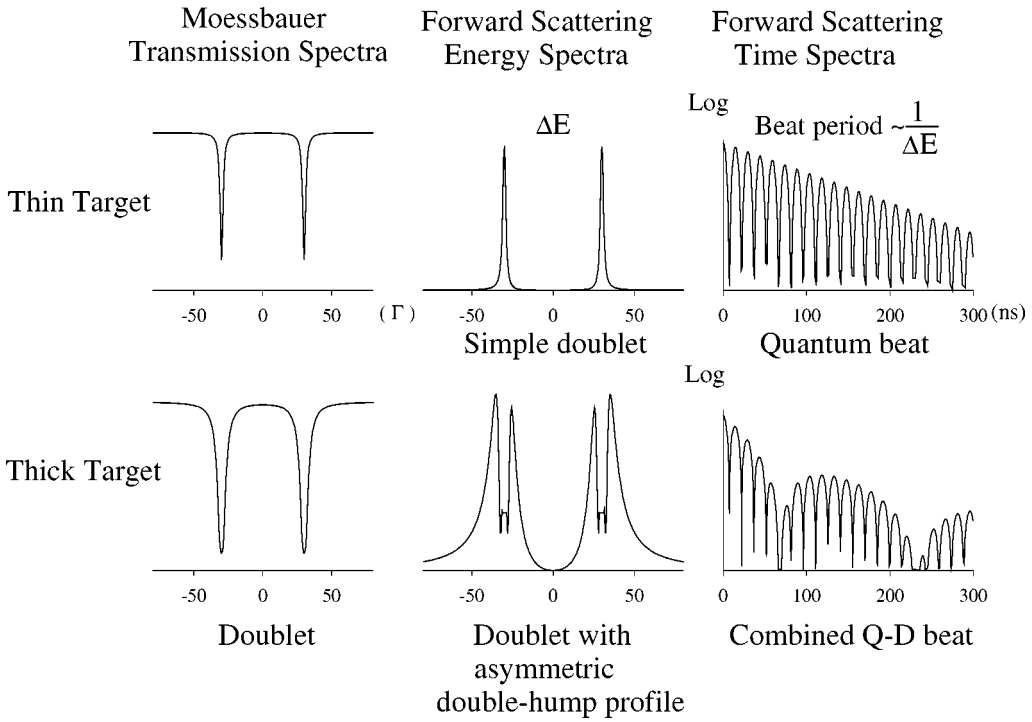

Figure 11. Mössbauer transmission spectra – left column, and synchrotron radiation scattering spectra in energy and time domain – middle and right columns, respectively, for the case of a resonance doublet in a thin target (0.2 μm thick ^{57}SS foil) – upper panel, and in a thick target (3 μm thick ^{57}SS foil) – lower panel.

case of splitting of the resonance is modulated in time: the nuclear exciton periodically flashes and is attenuated by decay (figure 11, lower right).

By measuring the quantum beat frequency one can immediately determine the energy separation of the nuclear transitions. However, the complexity of a quantum beat pattern grows drastically with increasing number of interfering transitions: $N_{\mathrm{F}} = N_{\mathrm{T}}(N_{\mathrm{T}}-1)/2$, where N_{F} is the number of frequencies in the beat pattern and N_{T} is the number of transitions. A preliminary knowledge of the energy spectra as provided by traditional Mössbauer spectroscopy should be involved to fit the quantum beat spectra in these cases. But it does not mean that a time spectrum simply confirms what is known from a traditional Mössbauer measurement. The Mössbauer timing experiment has its essential merits and advantages (see [11,34]), which are provided on the one hand by the unique properties of SR: superior spatial and angular density of radiation, high degree of polarization, etc., and on the other hand, by the principal difference in the techniques of measurements. In the traditional Mössbauer experiment the phase relation between the frequency components of the radiation is lost. Therefore only the strengths of the frequency components are revealed in an ordinary spectroscopic method. Because of the phase corellation between the frequency components the time

measurement presents an interferometric technique rather than a spectroscopic one. Therefore a quantum beat like an interference pattern is very sensitive to the relative strengths of the frequency components of the resonance and to a slight variation of the hyperfine interaction parameters, including the orientation of the hyperfine fields. The latter aspect we consider in section 6.8 while regarding the transmission of SR through an optically active resonant medium. But first let us briefly analyze the case of resonant splitting in a thick target.

6.6. Combined dynamical and quantum beats

We consider again a symmetric well resolved resonant doublet. In this case the solution of the wave equation for an optically thick target results in the FS energy spectrum displayed in figure 11 lower panel. The spectrum is drastically changed compared to that of an optically thin target. The double-hump profiles are formed at each resonance, as described in section 6.4, but now each profile is not symmetric due to the mutual influence of the resonances. The reason is as follows. The real parts of the susceptibilities of the two resonances are added. In the frequency range between the resonances, which is the right-hand side of one resonance and the left-hand side of the other, they have opposite signs (see figure 1(c)). Therefore, in this range destructive inter-resonance interference occurs. And vice versa, constructive interference takes place in the outer frequency range. Thus, the inter-resonance interference gives rise to an asymmetry of the double-hump profiles.

The time evolution of the forward scattering in this case exhibits both quantum and dynamical beats (figure 11 lower right). However, the QB period does not correspond to the energetic separation of the resonances. The QB are faster because due to the asymmetry of the double-hump profiles the centers of gravity of the profiles are shifted towards higher frequencies. Dynamical beats are less pronounced due to the asymmetric shape of the double-hump structure. The outlined tendencies develop as the separation of the resonances decreases. The profiles become more and more asymmetric until the inner maxima disappear. Approaching this limit the QB and DB can not be identified separately [35]. When the resonances finally coincide dynamical beats corresponding to the doubled strength of the resonance are formed.

As demonstrated in [36] the inner humps specific for a thick target can be completely smeared out even at a large distance between the resonances. This happens in an Invar alloy due to inter-resonance interference in the case of an asymmetric distribution of the magnetic hf fields. The beats observed in this case are called *hybrid beats*.

Thus, in transmission of a SR pulse through a resonant target the delayed wave packet is generated as a response of the nuclear ensemble. It can have a complicated node–antinode structure due to inter-resonance interference and due to multiple scattering of the resonant γ-ray through the target.

6.7. Resonance broadening and probability of coherent and incoherent emission

Due to the interaction of a nucleus with its environment in the target the nuclear state may change from site to site over the ensemble of nuclei and even vary at a site during the collision time. This gives rise to inhomogeneous or homogeneous broadening of the nuclear resonance. The broadening of the resonance has an influence on the time evolution of SR nuclear scattering both in the coherent (see, e.g., [13,27, 36]) and the incoherent scattering [27] channels. Regarding the coherent scattering channel one has to average the scattering amplitude over the nuclear ensemble. If the Lorentzian shape of the resonance is preserved one ends up with the response function of the nuclear forward scattering given by eq. (6.13) and with the relevant intensity, eq. (6.14). The broadening factor q, see eq. (6.4), leads to an accelerated decay of the coherent signal, with the integral coherent intensity decreased (in contrast to speeded up decay due to enhancement of the radiative channel, where the integral intensity is enlarged). It is of interest to analyze the re-distribution of the scattering intensity in the full picture of scattering, including both coherent and incoherent channels.

We assume that the field scattered over 4π originates only from scattering of a strong coherent wave. Considering the delayed field scattered over 4π one can distinguish three scattering paths of the coherent field propagating into the forward direction:

A – recoilless nuclear scattering of the prompt and delayed parts of the radiation,

B – nuclear scattering with recoil of the prompt part of the radiation,

C – elastic electronic scattering of the delayed part of the radiation.

We rewrite the expressions for the A, B, C contributions obtained in [27]:

$$
\begin{aligned}
I^{\mathrm{A}}_{4\pi}(z,\tau) &= \frac{I_0}{\Delta\omega t_0}\frac{\Gamma_{\mathrm{e}}}{\hbar} n\sigma_0\beta f_{\mathrm{LM}} \mathrm{e}^{-\mu_e z} \\
&\quad \times \int \frac{\mathrm{d}\widetilde{w}}{\pi}\frac{W}{\widetilde{w}^2+W^2}\left|\int \frac{\mathrm{d}w}{2\pi}\frac{\exp(-\mathrm{i}w\tau)}{w-\widetilde{w}+\mathrm{i}/2}\exp\left(-\mathrm{i}\frac{\mu_n z}{2(2w+\mathrm{i}q)}\right)\right|^2, \\
I^{\mathrm{B}}_{4\pi}(z,\tau) &= \frac{I_0}{\Delta\omega t_0}\frac{\Gamma_{\mathrm{e}}}{\hbar} n\sigma_0\beta(1-f_{\mathrm{LM}})\mathrm{e}^{-\mu_e z}\mathrm{e}^{-\tau}, \\
I^{\mathrm{C}}_{4\pi}(z,\tau) &= n\sigma_{\mathrm{photo}} I_{\mathrm{fs}}(z,\tau),
\end{aligned}
\tag{6.21}
$$

where $W = (q-1)/2$, $w = \hbar(\omega-\omega_0)/\Gamma$, and $\widetilde{w}$ is the parameter of the resonant energy distribution. The scattering intensities should now be averaged over the energy distribution of the resonance in the nuclear ensemble (see the first equation in (6.21)) rather than the amplitudes as in the case of coherent scattering. The intensities given by eqs. (6.21) should be summed and integrated over the target thickness to get the total intensity of incoherent scattering (here the fluorescent scattered radiation is regarded).

The intensity of the forward and the incoherent scattering represents the time differential probability of the emission of a secondary particle. *We here introduce the*

probability of emission as a function of time which is the integral $P(t) = \int_0^t \mathrm{d}t' I(t')$. The evolution of the relevant emission probabilities $P_{\mathrm{fs}}(t)$ and $P_{4\pi}(t)$ is given in figure 12 for a single line resonant target equivalent in thickness to a fully enriched 1 μm thick SS foil, for two resonance widths 2Γ and 10Γ. Obviously, *the sum of* $P_{\mathrm{fs}}(t)$ *and* $P_{4\pi}(t)$ *yields the decay probability of the nuclear exciton*.

The following messages can be obtained from figure 12. In the coherent channel the broadening of the resonance leads to a slowing down of the emission probability growth and to a large lowering of the final probability level. In the incoherent channel the effect of resonance broadening is just opposite – a more rapid rise of the emission probability is observed and a much higher level of the final probability is reached. It is of interest to see how the balance between the channels develops. At early times the nuclear exciton decays predominantly into the forward direction, the coherent emission exceeds the incoherent one in this time interval. However, the probability of coherent emission gets saturated much earlier, somewhere between 40 and 100 ns depending on the width of the resonance. After this time interval the nuclear exciton continues to decay predominantly in the incoherent channel. The probability of decay in this channel rises much slower and only saturates after 400 ns.

The probability of coherent emission at $t \to \infty$ decreases due to resonance broadening, whereas the probability of the incoherent decay increases essentially with the width of the resonance, so that the total probability at $t \to \infty$ should not depend on the resonance width.

Up to now we considered the frequency composition of the forward scattered packet and its time evolution for some characteristic cases without taking into account a possible optical anisotropy of the target. Meanwhile optical anisotropy and optical

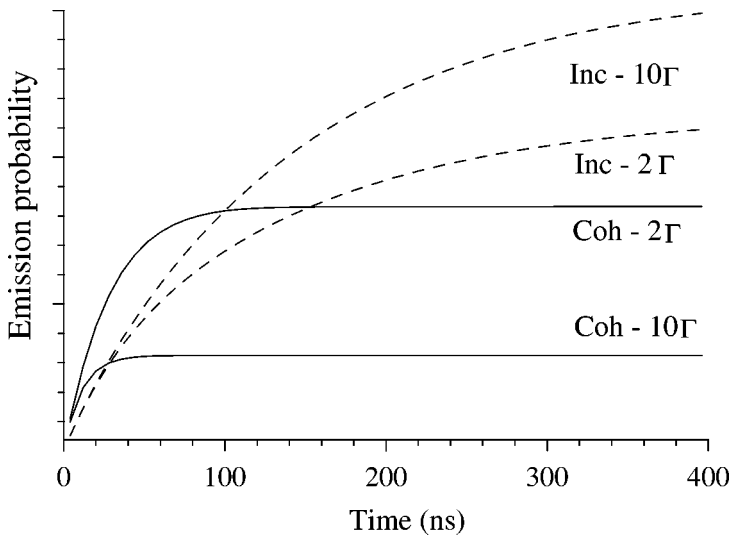

Figure 12. Time evolution of the probability of emission in the coherent and the incoherent channels for different resonance broadenings.

activity of the nuclear medium strongly influence the polarization state of the radiation. In the following subsection we shall consider polarization effects.

6.8. *Propagation of SR through an optically anisotropic and active medium, polarization effects*

A nuclear medium with preferred orientations of hyperfine magnetic fields or of electric field gradients becomes optically anisotropic for the resonant radiation and exhibits optical activity. The incident unpolarized radiation can get polarized, or if the incident radiation is polarized it can drastically change its polarization state. The field in a medium is obtained by the solution of the following set of dynamical equations:

$$\begin{aligned}\left(\frac{k^2}{K^2}-1\right)E^\sigma &= \eta^{\sigma\sigma}E^\sigma + \eta^{\sigma\pi}E^\pi,\\ \left(\frac{k^2}{K^2}-1\right)E^\pi &= \eta^{\pi\sigma}E^\sigma + \eta^{\pi\pi}E^\pi,\end{aligned} \tag{6.22}$$

where the nuclear susceptibility amplitudes $\eta^{ss'}$ with $s, s' = \sigma, \pi$ form a matrix of second rank under these conditions, the elements of which determine the probability amplitudes for the transitions between σ and π polarized states. As a function of frequency the susceptibility has several resonances in the range of hyperfine interaction. Equation (6.22) represents a set of two homogeneous linear equations for the scalar amplitudes of the field. Setting its determinant equal to zero to obtain the nontrivial solution yields a second order equation for k with two solutions k_1 and k_2. So the general solution for the transmitted wave is

$$\mathbf{E}_{\rm tr} = E_0 \cdot \mathrm{e}^{\mathrm{i}\omega t}\left(\mathbf{e}_1 \cdot \mathrm{e}^{-\mathrm{i}k_1 z} + \mathbf{e}_2 \cdot \mathrm{e}^{-\mathrm{i}k_2 z}\right) \tag{6.23}$$

with

$$\mathbf{e}_1 = \mathbf{e}^\sigma E_1^\sigma + \mathbf{e}^\pi E_1^\pi \quad \text{and} \quad \mathbf{e}_2 = \mathbf{e}^\sigma E_2^\sigma + \mathbf{e}^\pi E_2^\pi,$$

where $\mathbf{e}^\sigma$ and $\mathbf{e}^\pi$ are the unit electric polarization vectors oriented along the x- (vertical) and y-axes, E_i^s is the scalar wave amplitude and k_i is the z-projection of the wave propagation vector.

Thus, the total wave in the medium consists of two partial fields, WF1 and WF2, each experiencing its own refraction while propagating through the medium. In turn the WF1 and the WF2 are *superpositions of the two orthogonal waves π and σ*. The polarization structure of the total field is shown schematically in figure 13 (we have chosen the same geometry as described in section 6.1). The propagation vectors and scalar amplitudes of the constituent waves are determined by the nuclear susceptibility amplitudes. The explicit solution of the problem of propagation of γ-radiation through an optically active medium is beyond the scope of the present paper, it can be found, e.g., in [37,38].

As a simple example we consider the illustrative case of scattering of SR by a thin ^{57}Fe target. The magnetic hyperfine interaction takes place in the ground and the

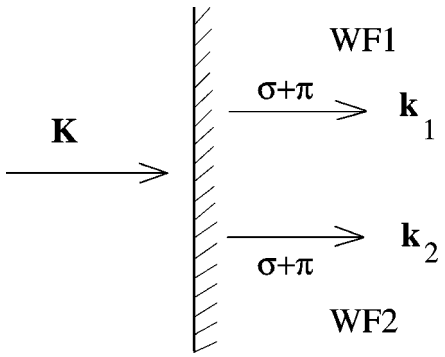

Figure 13. Transformation of an incident plane wave in an optically active medium.

first excited states of ^{57}Fe with spins $1/2$ and $3/2$, respectively. Due to the magnetic hyperfine interaction the nuclear levels are split into two sub-levels in the ground state and into four sub-levels in the excited state. The new states are pure $|m\rangle$-states with quantization axis parallel to the internal magnetic field; the magnetic quantum numbers are $m_{\rm g} = \pm 1/2$ and $m_{\rm e} = \pm 1/2, \pm 3/2$. By the selection rules six transitions between the sub-levels of the ground and excited states with $\Delta m = m_{\rm e} - m_{\rm g} = 0 \pm 1$ are allowed.

Polarized SR makes possible selective excitation of different groups of nuclear transitions. In figure 14 the polarization of SR and the scattering geometry are shown.

A simple practical rule for the selective excitation of a magnetic dipole transition is the following: *the magnetic polarization vector* **h** *of the incident wave should have a component along the magnetic hyperfine field* $\mathbf{H}_{\rm hf}$ *in order to excite* $\Delta m = 0$ *transitions and it should have a component perpendicular to* $\mathbf{H}_{\rm hf}$ *to excite* $\Delta m = \pm 1$ *transitions*. Let us consider the orientations of $\mathbf{H}_{\rm hf}$ along the axes x, y, z. With $\mathbf{H}_{\rm hf} \| y$ only the lines 2 and 5 are excited. In this case the solution for the wave packet scattered by a thin target is

$$\begin{aligned} &\text{in the energy domain} \quad \mathbf{E}_{\rm fs}(\omega) \propto E_0 \mathbf{e}^{\sigma} \left[R(\omega - \omega_2) \mathrm{e}^{\mathrm{i}\omega_2 t} + R(\omega - \omega_5) \mathrm{e}^{\mathrm{i}\omega_5 t} \right], \\ &\text{in the time domain} \quad \mathbf{E}_{\rm fs}(t) \propto E_0 \mathbf{e}^{\sigma} \mathrm{e}^{-t/(2t_0)} \left(\mathrm{e}^{\mathrm{i}\omega_2 t} + \mathrm{e}^{\mathrm{i}\omega_5 t} \right) \end{aligned} \tag{6.24}$$

with $R(\omega)$ defined in eq. (6.18). The solution in the energy domain consists of two groups of identically linearly σ-polarized oscillations with carrier frequencies ω_2 and ω_5. The spectral compositions of the oscillation groups are shown in figure 15A (right bottom). The magnetic polarization vector of the scattered radiation and the hyperfine field are parallel, $\mathbf{h}^{\sigma} \| \mathbf{H}_{\rm hf}$. In the time domain one has two wave packets of the FS radiation at carrier frequencies ω_2, ω_5 and of the same polarization state. The interference between the groups in the energy domain or between the wave packets in the time domain gives rise to the quantum beats of the forward scattered radiation displayed in figure 15B (left bottom). The most simple beat pattern is realized in this case. The beat occurs at a single frequency, $\Omega_{5,2} = \omega_5 - \omega_2$, and with

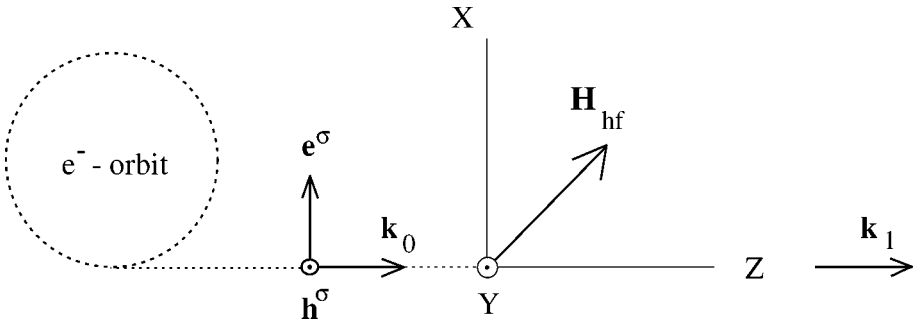

Figure 14. Polarization of synchrotron radiation, $\mathbf{e}^\sigma$ and $\mathbf{h}^\sigma$ are the electric and magnetic polarization vectors for a σ-polarized electromagnetic wave.

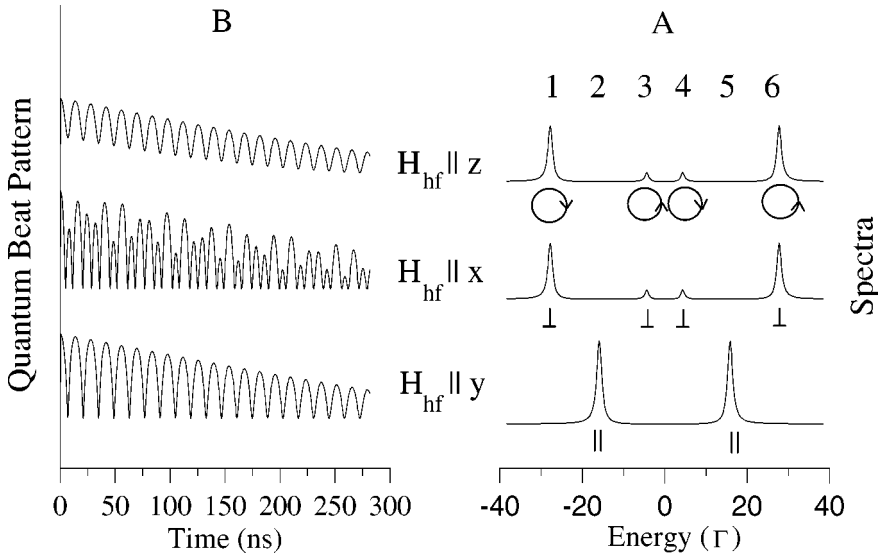

Figure 15. Spectral compositions (A) and time dependences (B) of nuclear forward scattering of SR by a 0.2 a μm thick ^{57}Fe foil for three different orientations of the foil magnetization (for the scattering geometry see figure 14).

the highest contrast since oscillators of equal strength interfere. The beat period is about 14 ns.

With $\mathbf{H}_{\rm hf} \| x$, only $\Delta m = \pm 1$ transitions are excited, i.e., the lines 1, 3, 4, 6. The forward scattered radiation is σ-polarized as in the previous case, however the magnetic polarization vector and the hyperfine field are perpendicular, $\mathbf{h}^\sigma \perp \mathbf{H}_{\rm hf}$. The solution has the same form as given by eq. (6.24) but it now contains four groups, four wave packets, at the frequencies $\omega_1, \omega_3, \omega_4, \omega_6$. The oscillation strengths are $3:1:1:3$ in this case. The corresponding spectral composition and the beat pattern are shown in the middle panel of figure 15. The interference of the four groups of oscillations yields a more complicated quantum beat pattern which now contains

four beat frequencies (although the number of possible beat frequencies is 6, see section 6.5) because in iron $\Omega_{3,1} = \Omega_{6,4}$ and $\Omega_{4,1} = \Omega_{6,3}$. The beating of highest frequency is caused by interference of the outermost lines 1 and 6 (the beat period is about 8 ns).

Finally, when $\mathbf{H}_{\rm hf} \| z$ the solution for the FS radiation has the following form in the energy domain:

$$\mathbf{E}_{\rm fs}(\omega) \propto E_0 \big\{ \left(\mathbf{e}^\pi + \mathrm{i}\mathbf{e}^\sigma\right) \cdot \left[3R(\omega-\omega_1)\mathrm{e}^{\mathrm{i}\omega_1 t} + R(\omega-\omega_4)\mathrm{e}^{\mathrm{i}\omega_4 t}\right] + \left(\mathbf{e}^\pi - \mathrm{i}\mathbf{e}^\sigma\right) \cdot \left[R(\omega-\omega_3)\mathrm{e}^{\mathrm{i}\omega_3 t} + 3R(\omega-\omega_6)\mathrm{e}^{\mathrm{i}\omega_6 t}\right] \big\}, \qquad (6.25)$$

and in the time domain

$$\mathbf{E}_{\rm fs}(t) \propto E_0 \mathrm{e}^{-t/(2t_0)} \big\{ \left(\mathbf{e}^\pi + \mathrm{i}\mathbf{e}^\sigma\right) \cdot \left(3\mathrm{e}^{\mathrm{i}\omega_1 t} + \mathrm{e}^{\mathrm{i}\omega_4 t}\right) + \left(\mathbf{e}^\pi - \mathrm{i}\mathbf{e}^\sigma\right) \cdot \left(\mathrm{e}^{\mathrm{i}\omega_3 t} + 3\mathrm{e}^{\mathrm{i}\omega_6 t}\right) \big\}. \qquad (6.26)$$

The same nuclear transitions are excited as in the former case, figure 15 top. But now the oscillations related to these transitions are circularly polarized. Those corresponding to 1 and 4 transitions are left circularly polarized while the other two are right circularly polarized. Quantum beats occur due to interference of oscillations having the same polarization state, i.e., of the oscillations related to the 1 and 4 transitions and of those related to the 3 and 6 transitions. Since in iron $\Omega_{4,1} = \Omega_{6,3}$ the beat pattern has a simple form with a single beat period of 14 ns. Note that the interference contrast in the top curve is less than that in the bottom one, because the amplitudes of the interfering oscillations are not equal, their ratio is 3 : 1 (see eq. (6.25)).

We wish to emphasize that the spectral compositions corresponding to the last two cases (where the 1, 3, 4 and 6 transitions are excited) are absolutely identical, while the time dependences of the nuclear forward scattering look quite different (compare top and middle panels in figure 15). Indeed, the frequency content of the radiation in both cases is the same, but the polarization of the radiation field in one case strongly differs from that of the other. The time measurement manifests the difference of the polarizations, being an interference technique, it is able to reveal the amplitude of the oscillation as a complex number. In contrast, a spectroscopic method gives only the absolute value of the amplitude.

It is of interest to consider the sum of left and right circularly polarized waves of equal amplitude, e.g., of those corresponding to the 1 and 6 transitions. One readily obtains

$$\left(\mathbf{e}^\pi + \mathrm{i}\mathbf{e}^\sigma\right) \cdot \mathrm{e}^{\mathrm{i}\omega_1 t} + \left(\mathbf{e}^\pi - \mathrm{i}\mathbf{e}^\sigma\right) \cdot \mathrm{e}^{\mathrm{i}\omega_6 t} = 2\left(\mathbf{e}^\pi \cos\frac{\omega_6-\omega_1}{2}t + \mathbf{e}^\sigma \sin\frac{\omega_6-\omega_1}{2}t\right) \cdot \mathrm{e}^{\mathrm{i}((\omega_6+\omega_1)/2)t}. \qquad (6.27)$$

This relationship shows that the sum of left and right circularly polarized waves of equal amplitude at different carrier frequencies yields a linearly polarized wave at the carrier frequency $(\omega_1 + \omega_6)/2$, where the polarization vector precesses around the propagation direction with the frequency $(\omega_6 - \omega_1)/2$. In our case the period of precession is about 16 ns. This time dependent Faraday rotation of the polarization

plane was observed in [14,39,50]. It was proposed to use such an optical activity of samples in combination with the polarization filtering technique to distinguish the resonant radiation from the non-resonant one and in this way to suppress the intensive prompt radiation propagating in the forward direction [40,41].

Concluding this section one can say that the time dependences of SR nuclear resonant scattering yield rich information about hyperfine interactions. More complicated cases of combined magnetic and electric quadrupole interaction, of combinations of several sets of hyperfine fields, etc. can be investigated.

7. The nuclear exciton in a separated target

7.1. Radiative coupling in spatially separated nuclear ensembles

When describing the evolution of a nuclear exciton in space and time (section 6.3) one has to regard a united system where the two sub-systems, the γ-ray field and the nuclear transition current, are dynamically coupled to each other. The system is developing in the space occupied by the nuclear ensemble even if the ensemble is split into several spatially separated targets. This occurs because the SR pulse traversing the separated targets creates in all nuclei spatially and temporally phased excitations. The spatial phasing allows the exciton which comprises all targets involved to decay coherently via radiative emission into the forward direction. Therefore, a target split into several slices placed one after another in the SR beam behaves exactly as an unsplit target from the point of view of the dynamics of γ-ray propagation through the nuclear ensemble (in the absence of a relative motion of the slices). However, the idea of spatial separation of a nuclear target offers interesting and beneficial applications.

The interesting possibility appears in a separated nuclear ensemble to modify a nuclear exciton in a controllable way by manipulating its parts. As an illustrative example let us consider the forward scattering of a SR pulse in a target split into two parts A and B (figure 16) with nuclei which exhibit a single resonance.

The SR pulse instantly creates a nuclear exciton extending over the two parts of the target with effective resonance thicknesses T_{A} and T_{B}. Let the incident radiation be presented by a δ-function, i.e., $E_0(t) \propto \varepsilon_{\omega_0}\delta(t)$. The wave E_{A} transmitted through

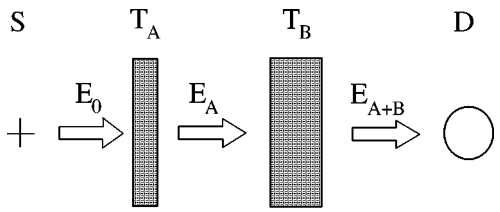

Figure 16. Set-up of a nuclear target consisting of two parts; T_{A} and T_{B} are the effective resonance thicknesses of the constituent targets, S and D are source and detector, E_0 represents the source radiation field, E_{A} and $E_{\mathrm{A+B}}$ represent the transmitted fields.

the first target and incident on the second target is given by eq. (6.13), where $\mu z = \mu d_{\mathrm{A}} = T_{\mathrm{A}}$ with d_{A} the physical thickness of target A. The field transmitted through the targets A and B is found as a convolution of field E_{A} and the time response function of target B (see eq. (3.6)):

$$E_{\mathrm{A+B}}(t) = \varepsilon_{\omega_0} \int_0^t \mathrm{d}t' \left[\delta\big(t-t'\big) - \frac{1}{2t_0} T_{\mathrm{B}} \cdot \mathrm{e}^{\mathrm{i}\omega_b(t-t') - q_b(t-t')/(2t_0)} \cdot \sigma\big(T_{\mathrm{B}}\big(\tau-\tau'\big)\big) \right] \times \left[\delta\big(t'\big) - \frac{1}{2t_0} T_{\mathrm{A}} \cdot \mathrm{e}^{\mathrm{i}\omega_a t' - q_a t'/(2t_0)} \cdot \sigma\big(T_{\mathrm{A}}\tau'\big) \right]. \tag{7.1}$$

In eq. (7.1) the second factor in square brackets represents the time dependence of the exciting field emerging from the upstream target, while the first factor in square brackets represents the response function of the downstream target (we omit the electronic absorption). The parameters ω_a, ω_b, and q_a, q_b are the resonance frequencies and the resonance broadening factors in targets A and B, respectively. While performing the integration we use $\int \mathrm{d}x \delta(x) f(a-x) = f(a)$, and obtain

$$E_{\mathrm{A+B}}(t) = \varepsilon_{\omega_0} \left\{ \delta(t) - \frac{1}{2t_0} \mathrm{e}^{\mathrm{i}\omega_b t - q_b t/(2t_0)} \left[T_{\mathrm{A}} e(t) \sigma(T_{\mathrm{A}}\tau) + T_{\mathrm{B}} \sigma(T_{\mathrm{B}}\tau) - \frac{T_{\mathrm{A}} T_{\mathrm{B}}}{2t_0} \int_0^t \mathrm{d}t' \mathrm{e}\big(t'\big) \sigma\big(T_{\mathrm{A}}\tau'\big) \sigma\big(T_{\mathrm{B}}\big(\tau-\tau'\big)\big) \right] \right\}, \tag{7.2}$$

where

$$\mathrm{e}(t) = \exp\left[\mathrm{i}(\omega_a - \omega_b)t - \frac{(q_a - q_b)t}{2t_0} \right], \qquad \tau = \frac{t}{t_0}.$$

The expression in the curly brackets of eq. (7.2) is the response function of the two-part target. We rewrite the response function as

$$R_{\mathrm{A+B}} = \delta(t) + R_{\mathrm{A}}(t) + R_{\mathrm{B}}(t) + R_{\mathrm{AB}}(t). \tag{7.3}$$

The scattering event is a coherent superposition of the four optical paths: transmission of the SR pulse without interaction with the nuclei, given by $\delta(t)$, nuclear scattering of the SR pulse by the upstream target, given by R_{A}, nuclear scattering of the SR pulse by the downstream target, given by R_{B}, and double nuclear scattering of the SR pulse first by the upstream and then by the downstream target, represented by R_{AB}. This last term represents the radiative coupling of the currents in target A with those in target B via the coherent field propagating in the forward direction. *Thus the response of the system is determined by the sum of responses of the constituent parts and of the term representing the radiative coupling of the parts*.

The role of radiative coupling is illustrated in figure 17. There the combined target consists of two stationary SS foils fully enriched in ^{57}Fe.

At the initial stage the response of the combined target is determined primarily by the sum of the responses of the targets A and B, i.e., by the interference of the wave packets E_{A} and E_{B} generated in the targets by the SR pulse. However, since

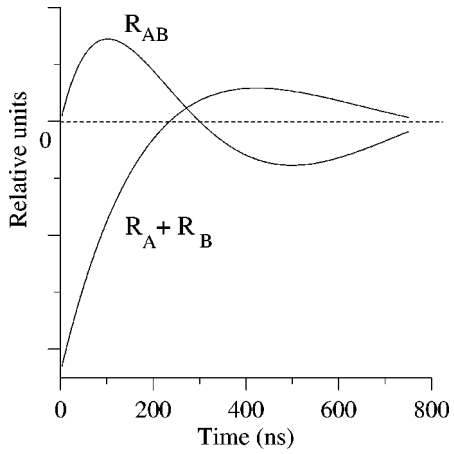

Figure 17. Comparison of the probability amplitudes of the scattering paths in separated targets (see figure 16). The targets A and B are 1 μm thick SS foils.

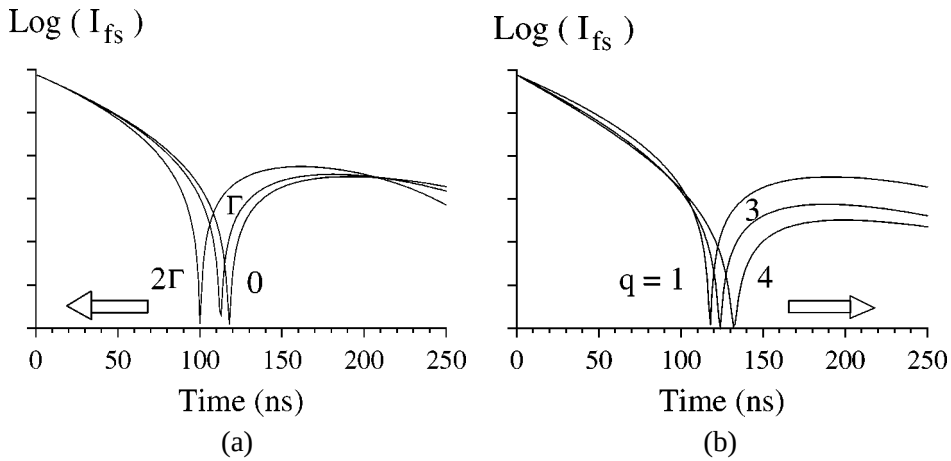

Figure 18. Time dependences of the scattering intensity from the target composed of two 1 μm thick SS foils at different separations of the resonance (a), and for different broadenings of the resonance in target A (b). Opposite shifts of nodal points of the dynamical beats are observed in cases (a) and (b).

the resonances in the targets coincide, the radiative coupling (or the interaction of the field E_{A} emerging from the upstream target A with the currents in the downstream target B) becomes essential. The relevant term rises quite rapidly after the excitation and reaches its maximum value at approximately the lifetime of the nuclear level. So the interference of the scattering paths considered above determines the delayed response of the combined target. As seen from figure 17, the interference between the packets $E_{\mathrm{A}} + E_{\mathrm{B}}$ and E_{AB} is mostly destructive during the decay time.

If a shift in energy between the resonances appears the role of radiative coupling rapidly decreases and a quantum beat between the wave packets E_{A} and E_{B} arises. The

impact of this kind of radiative de-coupling and quantum beat on the time dependence of the scattering intensity is displayed in figure 18(a). Initially a shift of the node of the dynamical beat to earlier times occurs (at higher separation of the resonances the nodes move towards later times). This effect was recently observed in [42]. The observed shift of the node of the dynamical beat could be a measure of the shift of the resonance in the sample relative to that in the reference target.

The broadening of the resonance in one target, say target A, also leads to a decrease of the radiative coupling of the targets A and B. However, the shift of the node of the beat occurs in opposite direction in this case, figure 18(b). Thus, in this way an unresolved splitting of a resonance could be distinguished from an inhomogeneous broadening.

7.2. On the commutativity of the target parts

It is quite obvious that targets A and B are commutative in the absence of their radiative coupling. Then the term R_{AB} in eq. (7.3) is simply zero and the rest of eq. (7.3) is independent on the sequence of targets. But it can be shown that the commutativity also holds when the targets are radiatively coupled, i.e., $R_{\mathrm{AB}} = R_{\mathrm{BA}}$. Indeed, the inversion of targets A and B results in mutual replacement of time variables in eq. (7.1): $t' \Leftrightarrow t - t'$. It can be readily checked that the same exchange of variables takes place in the integrand of eq. (7.2) and that the form of the wave packet $E_{\mathrm{A+B}}(t)$ is invariant to inversion of targets A and B. This is not obvious in the case where the thickness of the targets or the width of the resonances are different. It is because the exciting wave packet E_{A} and the exciton in downstream target B can be essentially different in the direct and inverted combinations of targets A and B.

Thus the commutativity is a universal property of the considered scattering geometry. One can show that it also holds when a dynamic perturbation, homogeneous in space and time, of the nuclear exciton in one of the targets, such as ultrasound (see, e.g., [46]) or magnetic rf excitation, takes place.

7.3. Time domain interferometry in a nuclear target consisting of two parts

If one foil is moved with respect to the other so that the resonances are completely separated energetically the radiative coupling vanishes. In this limit the response of the composite target is only determined by the interference of the wave packets E_{A} and E_{B} emitted by targets A and B. In the full de-coupling conditions one wave packet can serve as a reference packet to probe the phase and the amplitude of the other. In figure 19 the result of interference of the reference wave packet generated in a 0.5 μm thick SS foil and that generated in a 3 μm SS foil is shown as an illustration. The calculations are performed with the use of eq. (7.2).

As seen in figure 19, in the time window of observation the reference wave E_{A} exhibits no dynamical beat while the probed wave packet E_{B} exhibits a pronounced beat due to multiple nuclear scattering of radiation in the 3 μm thick target (see sections 6.2, 6.3). Two nodes and three antinodes are seen in the dynamical beats of

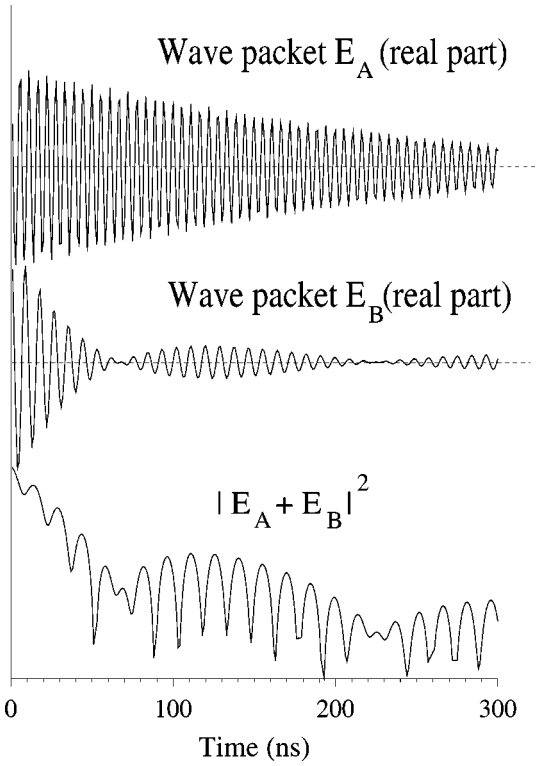

Figure 19. Probing of the amplitude and phase structure of the wave packet $E_{\rm B}$ (emitted from a 3 μm thick SS foil) with the help of the reference wave packet $E_{\rm A}$ (emitted from a 0.5 μm thick SS foil).

the wave packet $E_{\rm B}$. In passing the nodes of the wave packet phase inversion of the carrier oscillation occurs: the adjacent oscillations are mirror reflected in phase. When the carrier frequencies of the wave packets $E_{\rm A}$ and $E_{\rm B}$ are different the interference of wave packets leads to a quantum beat (see section 6.5). In our example the carrier frequencies of the interfering wave packets are $\omega_{\rm A} = 160$ and $\omega_{\rm B} = 100$ in relative units, so that in the interference pattern, the bottom panel in figure 19, quantum beats occur at the difference frequency $\Omega = 60$. It is well seen that the interference pattern reveals both the node–antinode structure of the probed wave packet $E_{\rm B}$ and the phase inversion in the node points of this packet [43,44]. As can be seen, a spatially separated target suggests a good opportunity to perform interferometric measurements.

The scheme shown in figure 16 can be modified by putting in-between targets A and B a nonresonant coherent scatterer, a sample target S, which changes the propagation direction of the wave train $E_{\rm A}$ (see figure 20). This can be done by employing as target S a Bragg scatterer or a total reflecting mirror or some other scattering system. In the modified scheme target B is put on the reflected beam.

The forward scattering in this target occurs in a new direction. In the scheme considered the prompt δ-function part of the SR radiation also creates a nuclear exciton in targets A and B. Of interest is that the wave train $E_{\rm A}$ is transformed into the wave

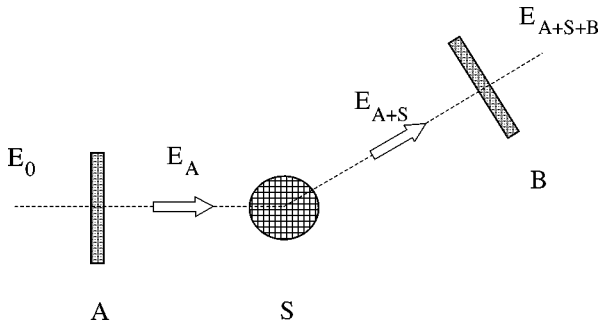

Figure 20. Modified scattering scheme for a separated nuclear target A + B. Between the parts of the nuclear target as the interferometer arms a sample electronic scatterer S is placed, which scatters coherently. Modulation of the wave packet due to slow atomic dynamics in S can be revealed by the nuclear interferometer.

train $E_{\mathrm{A+S}}$ which can be phase and amplitude modulated due to a possible dynamics in target S and then probed with reference wave E_{B}. Targets A and B can be regarded in this case as nuclear interferometer arms.

The interference arrangements shown in figures 16 and 20 were used in experiments: in [45,46] for studying the perturbation of the nuclear exciton by ultrasound, in [47] for phase modulation of the packet E_{A} with a vibrating nonresonant scatterer (piezo-quartz crystal), in [48] for the investigation of quasi-elastic coherent scattering in a diffusive target S (glycerol), in [49,51] for Mössbauer heterodyne spectroscopy.

In conclusion, we can say that useful time domain interferometry schemes can be constructed with the use of a two-part resonant target where one part creates a reference wave. With the help of the reference wave the amplitude and phase of the wave packet scattered by the other target can be probed.

8. Summary

The impact of ideas of coherent scattering on the art and science of Mössbauer spectroscopy became essential with the arrival of synchrotron radiation (SR). The coherent properties of the radiation and of the scattering mechanism are clearly demonstrated in a regular measurement with SR. Both the temporal coherence in scattering of a γ-ray by a single nucleus and the spatial coherence in scattering by a nuclear ensemble play a crucial role in the formation of the scattered wave field.

A scattering event is described as sequential absorption and re-emission of a γ-ray by nuclei. In accordance with the superposition principle the intermediate state of the nuclear excitation has to be regarded as delocalized over the nuclear ensemble where an exciting γ-ray is shared by nuclei. The spatial and temporal phasing of the excited nuclear currents over a system is determined by the space and time coherence of the field associated with the incident γ-ray. The superposition state of the nuclear excitations, called *nuclear exciton, became a central concept of the theory of nuclear*

resonant scattering. In a wider view a *nuclear exciton should be considered as a united state of a γ-ray field and nuclear transition currents where the two subsystems are dynamically coupled to each other*. The nuclear ensemble thus behaves as a macroscopic resonator, the properties of which can differ qualitatively from those of individual nuclei. This is demonstrated in changes of the time and space distribution of nuclear decay products, in the redistribution of probabilities of the radiative and nonradiative channels of scattering. In all these changes coherence effects play a crucial role.

The existence of a distributed coherent nuclear excitation, the nuclear exciton, provides a physical basis for the use of macroscopic polarization in the Maxwell equations to treat the radiative effects of nuclei. The total field represents a coherent superposition of the waves allowed by a scattering nuclear system. The waves are dynamically coupled via nuclear currents feeding one another so that the total field must be considered as a single entity.

The SR sources provide an excellent opportunity to observe the time evolution of nuclear scattering. The stages of nuclear excitation and decay are well separated in time so that a nuclear scatterer exhibits free decay.

The time dependence of coherent scattering can be regarded as an interference pattern where the time harmonics of the scattered radiation interfere. In this presentation the decay of the scattered intensity is interpreted as a fading of the interference signal which is due to the frequency components of a single resonance becoming more homogeneously distributed in phase with time. When the radiation spectrum contains several components well separated in energy, e.g., due to hyperfine interaction, the interference between the components leads to *quantum beats* of the scattered intensity. *Quantum beats are, thus, an effect of inter-resonance interference*.

Coherent constructive addition of wavelets re-radiated by nuclei determines the physical nature of the *strong enhancement of the radiative channel of nuclear resonant scattering*, called *superradiance*. It is observed as a huge enlargement of the coherent scattering intensity, e.g., in Bragg diffraction from crystals, in total reflection from nuclear mirrors, and in forward scattering. The strong coupling of the nuclear transition currents with the resonant γ-ray field propagating through the nuclear ensemble results in a dramatic speed-up of the coherent re-emission of γ-radiation by the nuclei.

The forward scattering geometry has become widespread in experiments with SR like the transmission geometry in normal Mössbauer spectroscopy. The decay of a nuclear exciton in the forward direction is characterized by strong enhancement of the elastic scattering channel leading to the effects mentioned above. In addition, the decay of a nuclear exciton in the forward direction can be accompanied by multiple absorption and re-emission, i.e., multiple scattering of a γ-ray in its propagation through nuclear media. The wave packet of propagating radiation in this case acquires a pronounced antinode–node structure both in time and in space. The relevant modulation of the scattered intensity in time and in space is called *dynamical beat*. The number of beats in the observation window for a given target actually shows the number of scattering events of a γ-ray by nuclei in a target.

In the energy domain the solution for the forward scattered radiation yields a *spectrum with a double-hump structure* where two pronounced humps are built up symmetrically at the sides of the resonance due to resonant scattering of the SR frequency components in a thick nuclear target. One can interpret the dynamical beat as the result of interference of two well resolved groups of oscillations.

Resonant scattering of synchrotron radiation by nuclei offers new possibilities to explore nuclear γ-resonance in matter. The new features of the experimental data originate from the coherent nature of scattering. The possibility to observe an interference pattern in space and in time makes the new technique complementary to Mössbauer spectroscopy. This is because an interference technique reveals the amplitude of the radiation field, say the amplitude of its electric field component, as a complex vector, while an absorption spectroscopy reveals only the strength of the radiation component. Vector properties of SR and optical anisotropy and activity of scattering media result in a wealth of polarization phenomena. Interesting applications of time domain interferometry are offered by the two-part resonance target where one part creates a reference wave.

Time differential measurements of nuclear forward scattering serve as a source of refined information about hyperfine interactions. By virtue of the interference nature of a quantum beat pattern it is usually more sensitive to distinguish relative strengths of the resonant components and a slight variation of the hyperfine interaction parameters including the orientation of the hyperfine fields. Complicated cases of combined magnetic and electric quadrupole interaction, of combinations of several sets of hyperfine fields, etc. can be investigated.

The time dependence of forward scattering also provides information on resonant broadening of both static and dynamic nature. They are usually better revealed in a measurement with a thin target. The forward scattering in a thick target yields a dynamical beat pattern which is very sensitive to the effective thickness parameters, in particular to the Lamb–Mössbauer factor.

We can only mention here that the time integral intensity of nuclear scattering measured as a function of variables like angle of incidence or scattering, sample temperature, magnetization, thickness, incident radiation energy, etc. can provide considerable information characterizing the scattering system. Detailed information concerning the spatial structure of the internal crystalline fields can be obtained by studying nuclear Bragg scattering.

Acknowledgements

The author is grateful to S.L. Popov, U. van Bürck, W. Potzel and P. Schindelmann for critical reading of the manuscript and valuable comments. The work was supported by the INTAS-RFBR International Scientific Program, reference number 95-0586.

References

[1] G.T. Trammell, in: *Proc. of Internat. Atomic Energy Agency Symp. on Chemical Effects of Nuclear Transformations*, Prague, 1960, Vol. 1 (IAEA, Vienna, 1961) p. 75.
[2] Yu. Kagan and A.M. Afanas'ev, in: *Proc. of Internat. Atomic Energy Agency Symp. on Mössbauer Spectroscopy and its Application* (IAEA, Vienna, 1972) p. 143.
[3] G.V. Smirnov, Hyp. Interact. 27 (1986) 203.
[4] U. van Bürck, Hyp. Interact. 27 (1986) 219.
[5] H. de Waard, Hyp. Interact. 68 (1991) 143.
[6] G.V. Smirnov, Hyp. Interact. 72 (1992) 63.
[7] G.V. Smirnov and A.I. Chumakov, in: *Resonant Anomalous X-Ray Scattering*, eds. G. Materlik, C.J. Sparks and K. Fischer (Elsevier, Amsterdam, 1994) p. 609.
[8] E. Gerdau, R. Rüffer, H.D Rüter and J.P. Hannon, Hyp. Interact. 40 (1988) 49.
[9] J. Arthur, D.E. Brown, S.L. Ruby, G.S. Brown and G.K. Shenoy, J. Appl. Phys. 67 (1990) 5704.
[10] R. Rüffer, Synchrotron Radiation News 5 (1992) 25; in: *Synchrotron Radiation and Dynamic Phenomena*, AIP 258 (1992) p. 539.
[11] E. Gerdau and U. van Bürck, in: *Resonant Anomalous X-Ray Scattering*, eds. G. Materlik, C.J. Sparks and K. Fischer (Elsevier, Amsterdam, 1994) p. 589.
[12] J.P. Hannon and G.T. Trammell, in: *Resonant Anomalous X-Ray Scattering*, eds. G. Materlik, C.J. Sparks and K. Fischer (Elsevier, Amsterdam, 1994) p. 565.
[13] G.V. Smirnov, Hyp. Interact. 97/98 (1996) 551; in: *X-ray and Inner-Shell Processes*, AIP 389 (1997) p. 323.
[14] S. Kikuta, in: *Resonant Anomalous X-Ray Scattering*, eds. G. Materlik, C.J. Sparks and K. Fischer (Elsevier, Amsterdam, 1994) p. 635;
S. Kikuta, Y. Yoda, I. Koyama, T. Shimizu, H. Igarashi, K. Izumi, Y. Kunimune, M. Seto, T. Mitsui, T. Harami, X. Zhang and M. Ando, in: *X-ray and Inner-Shell Processes*, AIP 389 (1997) p. 351.
[15] W. Sturhahn, E.E. Alp, T.S. Toellner, P. Hession, M. Hu and J. Sutter, Hyp. Interact. 113 (1998) 57.
[16] A.I. Chumakov, J. Metge, A.Q.R. Baron and R. Rüffer, Phys. Rev. B 56 (1997) R8455.
[17] A.M. Afanas'ev and Yu. Kagan, Zh. Eksper. Teoret. Fiz. 52 (1967) 191 (English translation in Soviet Phys. JETP 21 (1967) 124).
[18] Yu. Kagan and A.M. Afanas'ev, Z. Naturf. A28 (1973) 1351.
[19] Yu. Kagan, this issue, section III-1.1.
[20] J.P. Hannon, this issue, section III-1.2.
[21] P.P Ewald, Ann. Phys. 49 (1916) 1; 49 (1916) 117; 54 (1917) 519; Acta Cryst. 11 (1958) 888.
[22] R.E. Holland, F.J. Lynch, G.J. Perlow and S.S. Hanna, Phys. Rev. Lett. 4 (1960) 181;
F.J. Lynch, R.E. Holland and Hamermesh, Phys. Rev. 120 (1960) 513.
[23] G.J. Perlow, Phys. Rev. Lett. 40 (1978) 896.
[24] P. Helisto, T. Katila, W. Potzel and K. Riski, Phys. Lett. 85 A (1981) 177.
[25] S.L. Popov, G.V. Smirnov, U. van Bürck and W. Potzel, Europhys. Lett. 28 (1994) 439.
[26] Yu.M. Kagan, A.M. Afanas'ev and V.G. Kohn, J. Phys. C 12 (1979) 615.
[27] G.V. Smirnov and V.G. Kohn, Phys. Rev. B 52 (1995) 3356.
[28] U. Bergmann, J.B. Hastings and D.P. Siddons, Phys. Rev. B 49 (1994) 1513.
[29] W. Sturhahn, K.W. Quast, T.S. Toellner, E.E. Alp, J. Metge and E. Gerdau, Phys. Rev. B 53 (1996) 171.
[30] G.V. Smirnov and Yu.V. Shvyd'ko, Zh. Eksper. Teoret. Fiz. 95 (1989) 777 (English translation in Soviet Phys. JETP 68 (1989) 444).
[31] U. van Bürck, this issue, section IV-2.1.
[32] G.T. Trammell and J.P. Hannon, Phys. Rev. B 18 (1978) 165; and B 19 (1979) 3835.
[33] E. Gerdau, R. Rüffer, R. Hollatz and J.P. Hannon, Phys. Rev. Lett. 57 (1986) 1141.
[34] R. Rüffer and A.I. Chumakov, Hyp. Interact. 97/98 (1996) 589.

[35] U. van Bürck, W. Potzel, P. Schindelmann, G.V. Smirnov, E. Gerdau, O. Leupold, Yu.V. Shvyd'ko and H.D. Rüter, Jahresbericht HASYLAB97 (1998).
[36] Yu.V. Shvyd'ko, U. van Bürck, W. Potzel, P. Schindelmann, E. Gerdau, O. Leupold, J. Metge, H.D. Rüter and G.V. Smirnov, Phys. Rev. B 57 (1998) 3552.
[37] M. Blume and O.C. Kistner, Phys. Rev. 171 (1968) 417.
[38] U. Bergmann, D.P. Siddons and J.B. Hastings, in: *Resonant Anomalous X-Ray Scattering*, eds. G. Materlik, C.J. Sparks and K. Fischer (Elsevier, Amsterdam, 1994) p. 619.
[39] D.P. Siddons, U. Bergmann and J.P. Hastings, Phys. Rev. Lett. 70 (1993) 359.
[40] D.P. Siddons, J.P. Hastings, U. Bergmann, F. Sette and M. Krisch, Nucl. Instrum. Methods B 103 (1995) 371.
[41] T.S. Toellner, E.E. Alp, W. Sturhahn, S. Zhang, M. Ando, Y. Yoda and S. Kikuta, Appl. Phys. Lett. 67 (1995) 1993.
[42] U. van Bürck, W. Potzel, P. Schindelmann, G.V. Smirnov, E. Gerdau, O. Leupold, Yu. Shvyd'ko and H.D. Rüter, Jahresbericht HASYLAB97 (1998).
[43] U. van Bürck, W. Potzel, P. Schindelmann, G.V. Smirnov, S.L. Popov, E. Gerdau, O. Leupold, Yu.V. Shvyd'ko and H.D. Rüter, Jahresbericht HASYLAB96 (1997) 881.
[44] G.V. Smirnov, U. van Bürck, W. Potzel, S.L. Popov, P.S. Schindelmann, E. Gerdau, O. Leupold, Yu.V. Shvyd'ko and H.D. Rüter, in: *ICAME '97*, Book of Abstracts, MO.T15.P06.
[45] G.V. Smirnov, U. van Bürck, J. Arthur, S.L. Popov, A.Q.R. Baron, A.I. Chumakov, S.L. Ruby, W. Potzel and G.S. Brown, Phys. Rev. Lett. 77 (1996) 183.
[46] G.V. Smirnov and W. Potzel, this issue, section IV-2.8.
[47] H. Jex, A. Ludwig, F.J. Hartmann, E. Gerdau and O. Leupold, Europhys. Lett. 40 (1997) 317.
[48] A.Q.R. Baron, H. Franz, A. Meyer, R. Rüffer, A.I. Chumakov, E. Burkel and W. Petry, Phys. Rev. Lett. 79 (1997) 2823.
[49] R. Coussement, S. Cottenier and C. L'abbé, Phys. Rev. B 54 (1996) 16003.
[50] D.P. Siddons, U. Bergmann and J.B. Hastings, this issue, section IV-3.2.
[51] R. Coussement et al., this issue, section VII-4.